ABSTRACT

Title of Dissertation:	IN-SITU INVESTIGATION OF LITHIUM DENDRITE GROWTH AND ITS INTERACTIONS WITH A POLYMER SEPARATOR IN A LITHIUM METAL CELL
	Lingxi Kong, Doctor of Philosophy, 2023
Dissertation directed by:	Prof. Michael G. Pecht, Department of Mechanical Engineering

Lithium dendrites are metallic structures that initiate and grow inside a lithium battery during charging. Lithium dendrite growth can negatively affect battery cycle life and safety. Observing the dendrite growth process and revealing its interaction with other components is necessary to improve battery safety. This study uses a transparent optical cell to directly observe the dendrite growth process, explore the lithium dendrite growth modes under various current densities, evaluate the interactions between the dendrite and separator, and explore the effect of electrolyte additives on dendrite growth behavior. The dendrite growth under different current densities showed the transition of dendrite morphologies from a dense structure to a porous structure. The examination of the dendrite-separator interaction regions showed that dendrites can deform and penetrate the separator. We show that additives can enhance the uniformity of lithium dendrite distribution compared with the dendrite formed in the electrolyte without additives.

IN-SITU INVESTIGATION OF LITHIUM DENDRITE GROWTH AND ITS INTERACTIONS WITH A POLYMER SEPARATOR IN A LITHIUM METAL CELL

by

Lingxi Kong

Dissertation submitted to the Faculty of the Graduate School of the
University of Maryland, College Park, in partial fulfillment
of the requirements for the degree of
Doctor of Philosophy
2023

Advisory Committee:
Professor Michael G. Pecht, Chair
Professor Lourdes G. Salamanca-Riba
Doctor Michael H. Azarian
Professor Hosam K. Fathy
Professor F. Patrick McCluskey
Professor Stanislav I. Stoliarov

Acknowledgements

First and foremost, I am extremely grateful to my supervisor, Prof. Michael G. Pecht, for his invaluable advice, continuous support, and patience during my Ph.D. study. His immense knowledge and plentiful experience have encouraged me in all the time of my academic research. I would like to thank Dr. Michael H. Azarian, Prof. Lourdes G. Salamanca-Riba, Prof. Hosam K. Fathy, Prof. F. Patrick McCluskey, and Prof. Stanislav I. Stoliarov for their guidance and help as my advisory Committee. I would also like to thank Dr. Michael David Osterman, Dr. Diganta Das, and Dr. Robert Guy Utter for their technical support in my study. I would like to thank my colleague Zhou He, Sahithi Maddipatla, and Lokesh Sangepu for their help in both study and life. I would like to thank all the members of the Center for Advanced Life Cycle Engineering (CALCE). It is their kind help and support that has made my study a wonderful time. I want to thank my friends Jian Zhou, Chaolun Zheng, Zhengyang Wang, Chen Gong, Xingfeng He, and Zijiang Yang for their support. Finally, I would like to express my gratitude to my parents. Without their tremendous understanding and encouragement over the past few years, it would be impossible for me to complete my study.

Table of Contents

List of Abbreviations

DEC: Diethyl carbonate

DMC: Dimethyl carbonate

EC: Ethylene carbonate

EMC: Ethyl methyl carbonate

FEC: Fluoroethylene carbonate

ISC: Internal short circuit

LSV: linear sweep voltammetry

NMR: Nuclear magnetic resonance

PC: Propylene carbonate

ppm: Parts per million

PTFE: Polytetrafluoroethylene

PS: Propane carbonate

SEI: Solid electrolyte interphase

SEM: Scanning electron microscopy

SN: Succinonitrile

UHMWPE: ultrahigh molecular weight polyethylene

VC: Vinylene carbonate

Chapter 1: Introduction

The lithium-ion battery has been the most widely used power source for portable devices. But the safety and reliability of lithium-ion batteries are being challenged by numerous incidents. One of the root causes of lithium-ion battery failure is the lithium dendrite growth, a major obstacle to ensuring sufficient battery cycle life and safety. Lithium dendrites attack the electrolyte and may lead to an internal short circuit (ISC) [1], resulting in thermal runaway [2] or catastrophic failure. The hazards of lithium dendrites are summarized in Figure 1.1. One example is the Samsung Galaxy Note 7 fire incident in 2016, which resulted in a mass recall of about 1 million units [3]. It is possible that battery defects caused lithium dendrite growth triggered a thermal runaway event and eventually caused the battery fire [4].

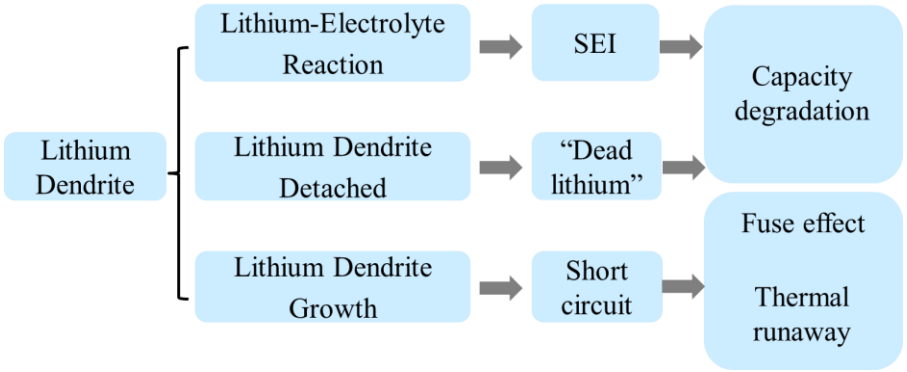

Figure 1.1 Lithium dendrite hazards. In this figure, SEI refers to the solid electrolyte interphase.

Lithium dendrites can affect the safe application of lithium-ion batteries and hinder the development of lithium metal-based rechargeable batteries. The performance and applications of the current lithium-ion battery are limited by its specific capacity. The graphite anode in the current commercial lithium-ion battery has a specific capacity of only 372 mAh/g [5], and the overall battery energy density is about 280Wh/kg [6]. Higher energy densities require a battery to operate with electrode materials with higher specific capacity or larger potential differences. Lithium metal can meet both requirements at the same time. This promising candidate has a specific capacity about ten times higher than graphite (3860 mAh/g) [7]. And the overall battery energy density can increase to 400-500 Wh/kg [6]. However, the lithium dendrite issue hinders the development of next-generation rechargeable lithium-ion batteries. The lithium dendrite formation and growth should be suppressed or removed first to develop a stable rechargeable lithium metal anode.

The lithium dendrite forms on the negative electrode (anode) during the charging process. The typical battery structure is shown in Figure 1.2. Inside a battery, if dendrite forms, the separator and electrolyte are in direct contact with it. The separator is a typical component that works as a mechanical barrier, and existing works showed that engineering the battery electrolyte property can alter the dendrite growth behavior. Understanding the mechanism of lithium dendrite evolution will aid in suppressing dendrite growth to enhance battery system safety and reliability. However, the battery is usually enclosed in a sealed case which is not transparent; direct dendrite growth observation is not enabled, and it is difficult to evaluate the relationship between

dendrite growth and influential factors such as current density, electrolyte additive, and separator.

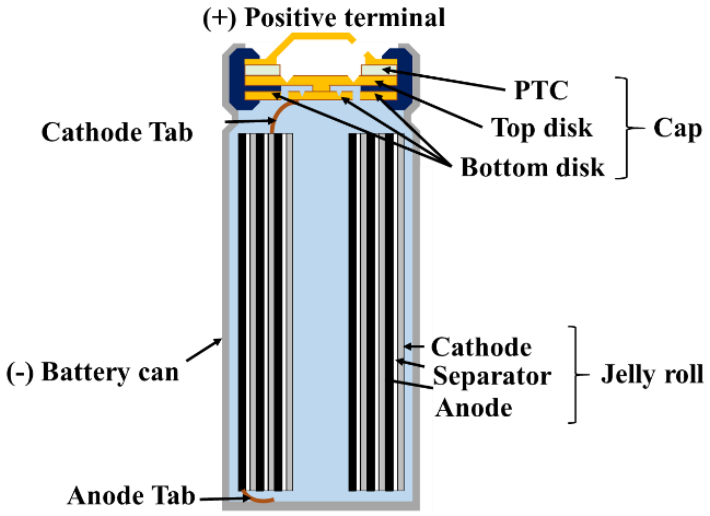

Figure 1.2 Cylindrical battery structure. In this figure, PTC refers to the positive temperature coefficient thermistor.

Chapter 2: Literature Review

Safety is a significant concern in electronic products powered by lithium-ion batteries, despite technological improvements in lithium-ion battery chemistry and design [8] [9]. One of the causes of thermal runaway, fires, and explosions is lithium dendrites [10] [11]. A lithium dendrite is a metallic microstructure formed on the anode and will grow toward the cathode, typically during battery charging. Once the dendrite connects two electrodes, it will let the current pass through, thus heating the surrounding organic materials and triggering an exothermic reaction, often leading to thermal runaway [12] [13].

Lithium dendrite is a metallic microstructure formed during the charging process—the lithium deposits on the negative electrode. Various terms were used in lithium dendrite research papers, such as "lithium plating [14]," "lithium deposition [9]," "dendritic growth [15]," and "filament [16]." In the literature, there are also other morphologies reported: "lithium needle [17]," "dendritic," "mossy [18]," and "arborescent like morphology [19]." The lithium plating is prone to grow in the dendritic format compared to other metal deposition processes [20]. These terms cover the observation results ranging in dimension from micrometer to millimeter levels. To make the experimental results from different battery systems comparable, Frenck et al. [21] suggested using normalized current density, which is the applied current density over the limiting current density.

Lithium dendrite growth is an electrochemical plating/deposition process. The current theory about lithium dendrite formation regarded this phenomenon as a direct result of nonuniform current distribution on the electrode. Due to the reactivity of lithium metal, when used in combination with non-aqueous electrolytes, a SEI layer covers the lithium electrode, a decomposition product from the electrolyte. Thus, the SEI and ion migration properties depend on the electrolyte. Since lithium-ion batteries work through the intercalation mechanism, the presence of metallic lithium metal is not desired. Depending on the morphology of the formed lithium dendrite, the localized stress and current density can be increased [22], [23]. Rechargeable lithium metal batteries work through the plating of lithium ion. Uniform plating is preferred over non-uniform plating (or dendritic plating). Figure 2.1 is a schematic illustration of the lithium dendrite growth within a symmetrical lithium metal cell. The gray parts correspond to lithium metal. The light green layer indicates the SEI layer and the dark green spots are locations with higher lithium ion flux. Dendrite growth occurs under several influential factors such as current density, electrolyte composition, separator, temperature, and charging profile. The response of lithium dendrite growth to these factors, such as the growth speed and the morphologies, are features to understand the lithium dendrite growth mechanisms.

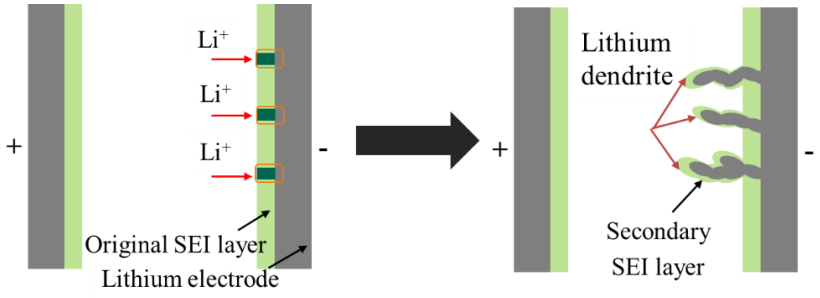

Figure 2.1 Local enhancement of Li ion flux.

2.1 Influential factors for lithium dendrite growth

The lithium dendrite morphology is influenced by various factors, which can be classified into thermodynamic and kinetic factors. The thermodynamic factors include temperature, surface energy, migration energy, and adsorption energy [24]. These factors relate to dendrite nucleation [25] and thermal relaxation [26]. Love et al. [27] showed the different dendrite morphologies under -10 °C, -5 °C, and 20 °C. Three different dendrite-separator interaction mechanisms were proposed. The kinetic factors include current density, ion diffusivity, electronic field, and charge transfer.

The methods for suppressing lithium dendrite growth involve regulating the environmental conditions and modifying electrodes, electrolytes, and separators. Various research groups have proposed methods for suppressing or blocking dendrite growth, such as the usage of anode coating [28], [29], composite polymer electrolyte [30], and concentrated electrolyte solution [31]. However, altering the battery materials alone does not guarantee complete suppression. Especially when the cycle number increases, the stability of the fine structure of the host material for lithium is questionable.

2.1.1 Temperature

In terms of temperature dependencies on dendrite growth, Love et al. [27] studied dendrite growth on symmetric Li cells in the electrolyte of EC: DMC (ethylene carbonate and dimethyl carbonate) with 1 M $LiPF_6$ at three ambient temperatures (–10, 5, and 20 °C). All three samples were charged using a constant current of 5 mA/cm^2. They observed dendrites having a mushroom-shaped structure at -10°C and a needle-

like shape at 5 °C and 20 °C. Aryanfar et al. [32] conducted constant charging tests on symmetric Li cells in the electrolyte of PC with 1 M $LiClO_4$ at 21, 48, and 70 ℃, respectively. Comparing the average dendrite lengths from all the three samples tested using a constant charge current of 2 mA/cm^2, they observed that dendrite grew more slowly at higher temperatures. They attributed this phenomenon to a thermal relaxation effect, which facilitates the diffusion of lithium atoms from the protruding part to the flat section. Akolkar [33] also mathematically models dendrite growth. The model-based simulation provides an estimate of the dendrite growth rate ratio, which is defined as the ratio of the localized current density at the dendrite tip to the current density of the flat electrode. When this ratio reaches a predetermined temperature threshold, the dendrite growth will transition from suppressed growth to uncontrolled dendritic growth. In a temperature range of -25 ℃~25 ℃, the author examined his model with the parameters of electrolyte EC: DMC with $LiPF_6$. The model is a function of current density ranging from 2 to 22 mA/cm^2, and the critical temperature gradually increases when the current density increases.

2.1.2 Current density

The effect of current density on dendrite growth rate was studied in the electrolyte of PC: DMC with 1 M $LiPF_6$ by Akolkar [34], who found that the dendrite growth rate can be estimated by the local current density at the dendrite tip, which is a function of flat surface current density and tip radius. Orsini et al. [35] conducted dendrite growth tests on three different types of electrodes: lithium, copper, and graphite, under galvanostatic conditions up to 2.6 mA/cm^2: 0.22, 0.45, and 0.9 mA/cm^2 for lithium; 0.45 and 2.6 mA/cm^2 for copper; less than 0.1 mA/cm^2 for graphite (exact value not

reported). Among their test results, increasing current density leads to the lithium dendrite morphology from “moss” (mossy) to “bulge” (shaper than mossy, but not dendritic) to “dendrite” (dendritic). Seong et al. [36] employed the “total amount of discharge” (discharge coulombs) as an indicator to quantify the current density effect on the lithium powder electrode. The electrolyte of EC: DMC with 1 M $LiClO_4$ was used, and samples were tested under galvanostatic conditions at 0.2, 0.5, 1, 2, and 5 mA/cm^2. Brissot et al. [19] studied the dendrite growth in symmetric lithium cells at 80 ℃ in the polymer electrolyte, which is the combination of poly(ethylene oxide) and $LiN(CF_3SO_2)_2$. Samples were tested under galvanostatic conditions at 0.03, 0.05, 0.1, and 0.7 mA/cm^2. According to the dendrite growth onset time difference, current densities were classified into two regions (separated at 0.18 mA/cm^2) where the formed dendrites have different morphologies.

2.1.3 Electrode

The negative electrode made of lithium metal will react immediately without charging with the surrounding electrolyte. In this process, an SEI layer will form at the interface. Compared with the graphite electrode, the lithium metal electrode is “hostless” [37]. The relative volume change of lithium metal electrodes is “virtually infinite” [38]. The huge volume change makes keeping a stable SEI layer on the lithium electrode challenging. Fresh lithium metal will be exposed to the electrolyte and continuously consume the electrolyte and reversible lithium content.

2.1.4 Electrolyte

The electrolyte is another battery component directly related to lithium dendrite growth. In the system of lithium metal negative electrodes combined with liquid electrolytes, the lithium dendrite is covered by an SEI layer. The SEI thickness is at the nanometer level [37]. The SEI layers are not uniform in either thickness or composition. The SEI layer properties depend on the electrolyte composition and the applied current density [39]. The electrolyte decomposition and SEI layer formation involve multiple steps [40].

The electrolyte is a mixture of organic solvent, lithium salt, and some additives [41]. The solvent of commercial lithium-ion batteries electrolyte has various choices, EC (Ethylene carbonate), DMC (Dimethyl carbonate), EMC (Ethyl methyl carbonate), and DEC (Diethyl carbonate) [42]. A compatible organic electrolyte is necessary for lithium metal-based rechargeable batteries in the future. The traditional aqueous electrolyte will already be decomposed because the lithium metal battery has a voltage higher than 4.0 V [43]. A counterexample is a battery with $Li_4Ti_5O_{12}$ anode material, which works at a lower voltage (higher potential on the anode side) and has no SEI layer formation or gaseous decomposition products [44]. The lithium salt used in the commercial electrolyte is usually $LiPF_6$. The commercial battery electrolyte usually contains additives other than pure solvent and a lithium salt, such as the SEI forming improver, cathode protection agent, lithium deposition improver, overcharge protection additives, flame retardant, and so on [45].

Electrolyte composition is expected to impact dendrite formation because it affects the composition of the SEI layer where dendrites initiate. Jeong et al. [31] found that the SEI formed in propylene carbonate (PC) electrolyte with higher $LiN(SO_2C_2F_5)_2$ concentrations can retard dendrite growth and improve cycling efficiency. Liu et al. [46] showed that their co-doped electrolyte could delay dendrite growth compared to other composite solid polymer electrolytes. Mogi et al. [47] tested the dendrite-blocking effect of PC-based electrolytes with different organic additives. They found that electrolytes with fluoroethylene carbonate (FEC) improved the battery life of the sample with the lithium-metal anode.

2.1.5 SEI

The SEI layer properties are dependent on the electrolyte composition. The electrolyte decomposition and SEI layer formation involve multiple steps [40]. Kim et al. [48] revealed the electrolyte decomposition process through a molecular dynamic simulation and varied their results with other experimental results. They studied the EC: DMC system, the electrolyte used in this study. In this system, the EC and DMC will generate the "radical anion" $LiOCO_2C_2H_4$, ($LiOCO_2CH_3$), and $LiOCO_2CH_3$ from the primary decomposition reaction. In the secondary decomposition process, Li_2CO_3, Li_2O, CO, Li_2CO_3, $LiOCH_3$, C_2H_4, LiEDC, and $LiOCO_2C_2H_4$ can be generated.

Due to the chemical reactivity of lithium metal, a non-aqueous organic electrolyte such as ethylene carbonate/dimethyl carbonate (EC: DMC) is used for the lithium metal system. The SEI thickness is at the nanometer level [37]. The SEI layer is a combination

of both organic and inorganic composite. The SEI layer's unevenness in thickness and composition can cause current redistribution near the lithium metal negative electrode. Various SEI compositions have been reported in research papers: $(CH_2OCO_2Li)_2$ [49], $ROCO_2Li$ [50], Li_2CO_3 [51], ROLi [52], LiF [53], Li_2O [54], polycarbonates [55], LiOH [56], $Li_2C_2O_4$ [57], and HCOLi [58]. The SEI layer substantially has a "mosaic" structure [59]. But a stable and uniform SEI is always preferred to improve battery safety and performance. Generally, the SEI compositions can be classified into organic and inorganic categories[60]. The organic part of the SEI layer is more permeable to the lithium ions [61], which makes the actual lithium ions flux distribution on the electrode surface not uniform. The spot with a higher flux will grow faster than the rest, leading to nonuniform lithium deposition or lithium dendrite growth [62]. The variance of the SEI composition is due to the multiple choices of the electrolyte and the electrolyte decomposition mechanisms.

2.1.6 Separator

In addition to electrolytes, the separator can also influence the lithium dendrite growth. Although the separator is not involved in the electrochemical reactions inside a battery, the separator has a porous structure containing micropores that interconnect to form the space to uptake the electrolyte and create a pathway for the ions. Mechanical and structural properties of a separator include thickness, porosity, layer number, puncture strength, tensile strength, and tortuosity [63]. Love theoretically analyzed the possible interaction modes between lithium dendrites and polymer separators at low

temperatures [64]. Through simulations, García et al. [65] pointed out that the dendrite-separator modes are coupled with current densities. Bai et al. [66] observed interactions between dendrite and nanoporous ceramic separators, showing that various lithium dendrite growth modes are current-dependent. The possible blocking effect of polymer separators on lithium dendrite growth is also worth investigating, especially through in-situ observation methods to reveal different growth modes. Alongside the study of separator material and structure, there is also research on improving the separator's function in detecting the lithium dendrite early. Cui et al. [67] developed a separator with a conductive layer embedded in the middle. Since the lithium dendrite can cause ISC, monitoring the voltage between the conductive layer and the negative electrode can detect the lithium dendrite growth. Existing studies regarded the separator as a rigid barrier blocking lithium dendrite growth. At the same time, the reverse effect of how the dendrite interacts with the separator is rarely mentioned.

2.2 Theoretical work

The theoretical work about lithium dendrite growth is still in development, especially a quantitative model that can accurately predict the lithium dendrite growth behavior still needs to be included. One of the reasons is that lithium dendrite is also electrically conductive and can continuously alter the geometry of the negative electrode. The other reason is that the lithium ion transportation in the lithium plating process is a multiphase transportation issue. Instead of Li^+ transportation in the pure liquid electrolyte phase, transportation in SEI is also essential.

The current theory about lithium dendrite formation regarded this phenomenon as a direct result of nonuniform current distribution on the electrode. However, the understanding of the dynamics of dendrite formation still needs to be improved. For instance, there is a debate about why the dendrite growth direction changes in the charging process. Nishida et al. [68] attributed this phenomenon to the accumulated residual stress in the dendrite growth process, while Steiger et al. [17] regarded the dendrite growth point changing as the reason. As noted, the previous work on dendrites growth involved electrolyte optimization and study on the temperature and current effects. The applied current densities are less than 3 mA/cm^2. However, in practice, the localized current density on the dendrite tip can reach up to 100 mA/cm^2 [34]. To evaluate dendrite growth mechanisms within a broader range of current density, higher current than the existing studies should be included.

Akolkar [34] developed a mathematical model describing the dendrite growth phenomenon during the charging process. In this model, the total overpotential on a flat lithium metal electrode includes the activation overpotential and the concentration overpotential, as described by the following equation:

$$\eta_f = \eta_{a,f} + \eta_{c,f} = \frac{RT}{\alpha_c F}\ln\left(\frac{i_f}{i_0}\right) - \frac{RT}{nF}\ln\left(\frac{C_e}{C_0}\right) \qquad \text{(eq. 2.1)}$$

Here the α_c is the cathodic transfer coefficient, i_0 is the exchange current density, and Ce is the lithium concentration at the electrode surface. Figure 2.2 is a schematic illustration showing the effect of lithium concentration at the electrode surface and applied current density on the overall overpotential.

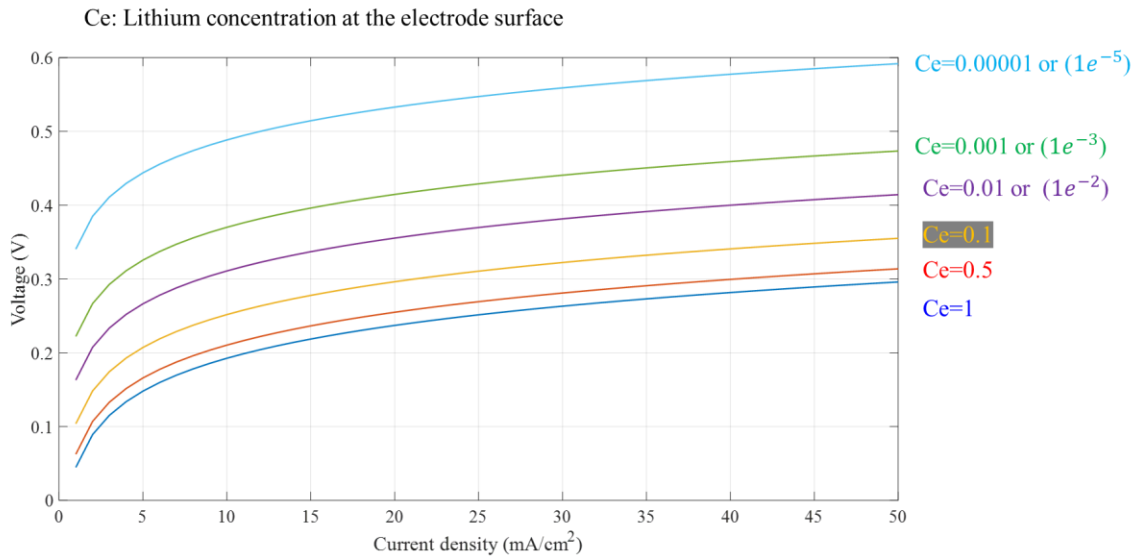

Figure 2.2 Lithium concentration at the electrode surface under various current densities and voltages.

With the dendrite growth, as illustrated by Eq.2, the local current density at the dendrite tip can be higher than the current density on the flat electrode. The relationship between the tip current density and the flat electrode current density is shown in the following equation:

$$\frac{RT}{\alpha_c F}\ln\left(\frac{i_f}{i_0}\right)+\frac{RT}{nF}\ln\left(\frac{C_e}{C_0}\right)+\frac{2\gamma K}{nFr}=0 \qquad \text{(eq. 2.2)}$$

Here the γ is the interfacial surface tension, K is the molar volume of lithium, and r is the radius of the lithium dendrite.

2.3 Observation of lithium dendrite

To observe the dendrite behavior, techniques such as scanning electron microscopy (SEM) [35] and nuclear magnetic resonance (NMR) [69] have been employed. However, these methods cannot provide in-situ monitoring to establish the relationship

between dendrite growth and electrical signals. Aryanfar et al. [70] developed a cylindrical-shaped optical sample to study "dead lithium" formation in the cycling process, but this type of cylindrical observation window causes image distortion and requires image pretreatment. Steiger et al. [17] constructed a micrometer-level optical sample to observe the behavior of a single dendrite in the cycling process. The dendrite growth direction change captured in their work was attributed to the growth point changing among the dendrite tip, bottom, and kink. However, the theory may not be suitable to explain the dendrite growth direction changing on a millimeter scale. Love et al. [27] implemented a dendrite observation using an optically transparent cell, which will avoid the weakness of the design in [70] and [17]. Our work follows the work of Love et al. with some improvements. In addition, we use the cell fixture to study additional cell parameters leading to dendrite growth.

2.4 Summary

The investigation of dendrites is challenging because their evolution is the result of a combination of different factors, including electrolyte composition [19], [31], [71], [72], ambient temperature [27][33][73], and current density [25], [34], [36], [68], [74]. The joint effects of these factors are expected to cause different lithium dendrite growth rates and morphologies. The process of dendrite evolution needs to be monitored to establish the relationship between dendrite growth and influential factors and to develop a predictive warning method. Typically, the current and voltage of a battery are monitored. However, these electrical signals will only show significant changes

once the dendrite growth causes an ISC. The current and voltage signals cannot be used to provide early warning to the dendrite-caused internal short circuit. Thus, a setup that can track the lithium dendrite growth process is needed to understand the lithium dendrite growth mechanisms.

Direct observation of the dendrite growth process is necessary to reveal the lithium dendrite growth mechanisms. The typical lithium-ion battery is enclosed in a sealed case which is not transparent, and only the electrical signals, such as current and voltage, can be measured. This limited the observation of lithium dendrite. A transparent cell was designed and assembled for this study to reveal the dendrite growth process and the corresponding mechanisms. This cell will allow continuous in-situ observation of the lithium dendrite growth process, capture real-time images, and collect the current and voltage signals. The samples used in this work are symmetrical lithium cells with two lithium metal electrodes as both the anode and cathode. Environmental conditions can influence the dendrite growth process. These influential parameters include the current density, temperature, and electrolyte composition. This study focuses on constant current charging to trigger dendrite growth.

2.5 Objects/motivation

For understanding the influence of lithium dendrite, a transparent cell allows the optical observation needed to track the evolution of dendrite growth under different current densities. This study will investigate dendrite growth based on experiments conducted using an optical cell for in-situ observations. By continuously monitoring the lithium

dendrite morphology and voltage evolution, the time of the first voltage drop can be identified, the dendrite growth rate can be estimated, and an early warning of failure can be given. Lithium dendrite growth tests under different current densities, various electrolyte additive concentrations, and separators with diverse structural properties can be used to explore potential engineering solutions for blocking or delaying the lithium dendrite growth process.

This work aims to reveal the root cause and mechanisms of lithium dendrite growth and investigate the environmental effects on the dendrite morphologies. This information can be used to prevent or mitigate lithium dendrite growth by removing the conditions favorable to dendrite growth. These efforts can improve the research of emerging lithium-based battery technologies.

The experiments will address three critical issues: the effect of current density during constant current charging on the lithium deposition morphology and growth rate, the impact of electrolyte additives on the lithium dendrite growth, and the interaction between lithium dendrite growth and the separator. The results can help determine lithium dendrite growth modes, growth mechanisms, and also the effectiveness of potential dendrite suppression methods.

Chapter 3: Experimental Setup and Materials

The sample is a “symmetrical cell” with two lithium metal electrodes. There are two electrolytes used in this study.

3.1 In-situ observation setup

Figure 3.1 shows the experimental setup used in this study. Part 1 is a symmetrical lithium metal optical cell. The dendrite growth will be induced in this sample. The sample is in connection with a battery tester (part 2). The tester will apply the current to drive the dendrite growth and record the electrical signals during the test. Part 4 is an example of electrical signals (current and voltage) collected from a previous test. Part 3 is a digital microscope connected to a desktop. The real-time dendrite images will be gathered and stored. Part 5 is an example of the dendrite morphologies corresponding to the electrical signals shown in part 4.

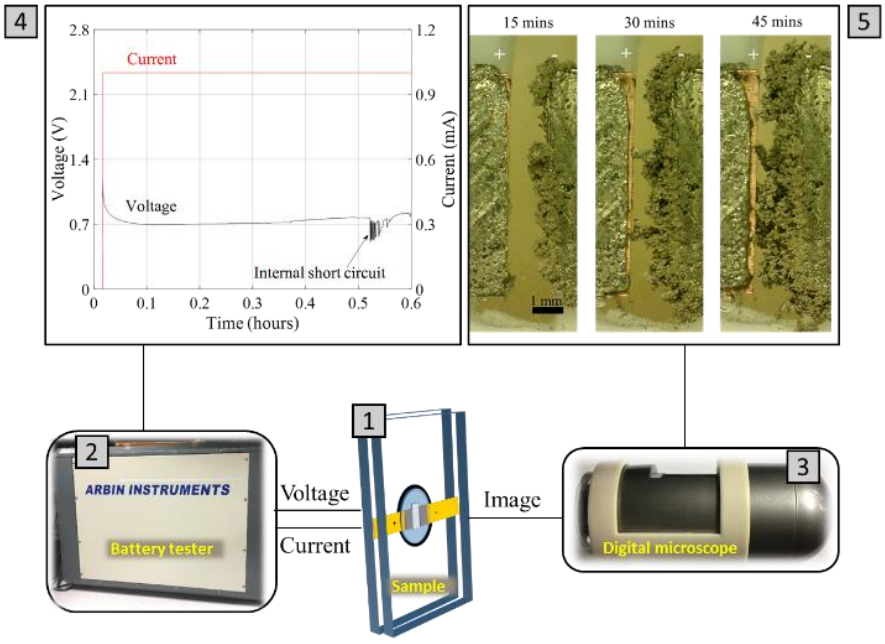

Figure 3.1 The experimental setup.

3.2 In-situ observation cell

Figure 3.2 shows the cell's schematic illustration for in-situ dendrite growth observation. This is a symmetric cell in which both the positive and the negative electrodes are made of lithium metal. The observation window is located in the center. The cell has several parts (Figure 3.3: No. 1–7). The plates on the top (No. 5) and at the bottom (No. 1), in combination with six screws, work as a fixture to hold the electrodes and the window. Round-shaped quartz windows (No. 2, 6) are put in the middle between two plates. An O-ring (No. 3) confines two lithium foils and a Teflon® disc (No. 4) between two quartz windows. Dendrite growth can be monitored through quartz windows.

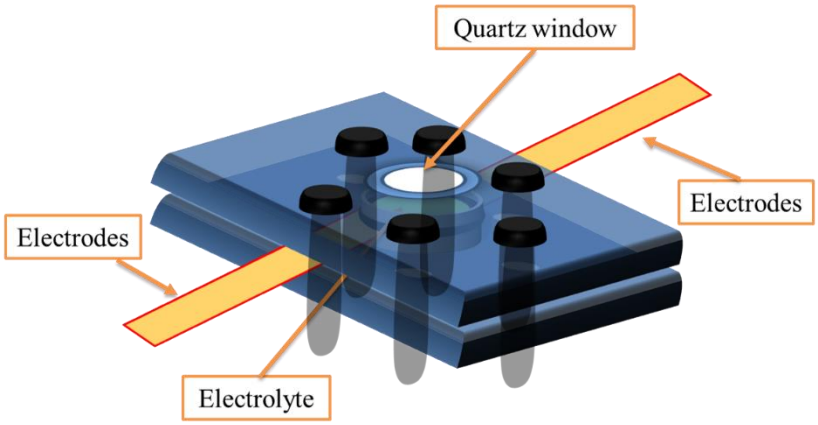

Figure 3.2 Sample for In-situ Observation.

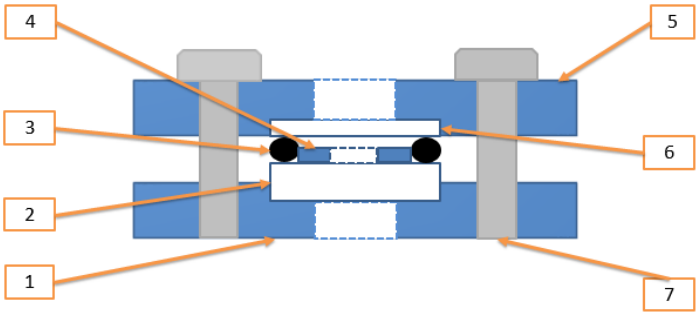

Figure 3.3 Side view of the quartz window cell with the fixture: (1) Bottom cell plate; (2) Quartz window; (3) O-ring; (4) Teflon® disc; (5) Top cell plate; (6) Quartz window; (7) Screws.

Figure 3.4 is a close look at the imaging collecting setup. Electrodes are made of lithium metal (gray) on top of the copper current collector (yellow). The electrodes are sandwiched between two transparent quartz windows. Between two windows, a white spacer made of polytetrafluoroethylene (PTFE) supports the electrodes. The spacer has an opening slot in the middle to provide space for more electrolytes. The circumferential direction is sealed with an O-ring (black).

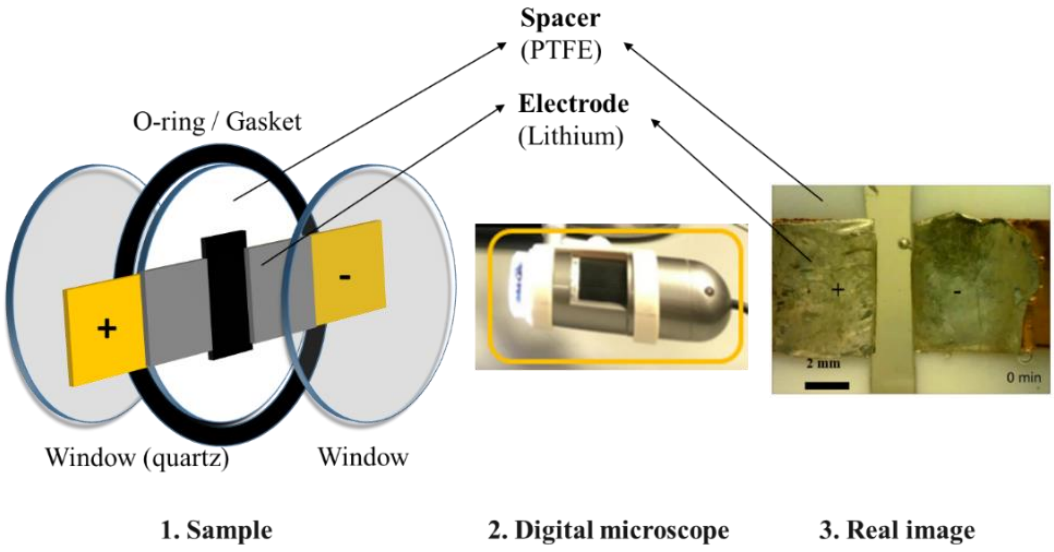

Figure 3.4 The imaging collecting setup.

3.3 Implementation of separator

In order to observe the dendrite growth process, especially the interaction between the separator and the dendrite, a piece of polymer separator was covered on the negative electrode by folding at the front edge of the negative electrode (Figure 3.5). The width of the electrode is about 5mm. The width of the separator is 15 mm. The sample was assembled in a glovebox filled with high-purity argon gas; the humidity and oxygen level were strictly controlled to below 1ppm. The assembled sample was transferred out of the glove box for electrical tests at room temperature. In the test process, the cell was charged with a constant current.

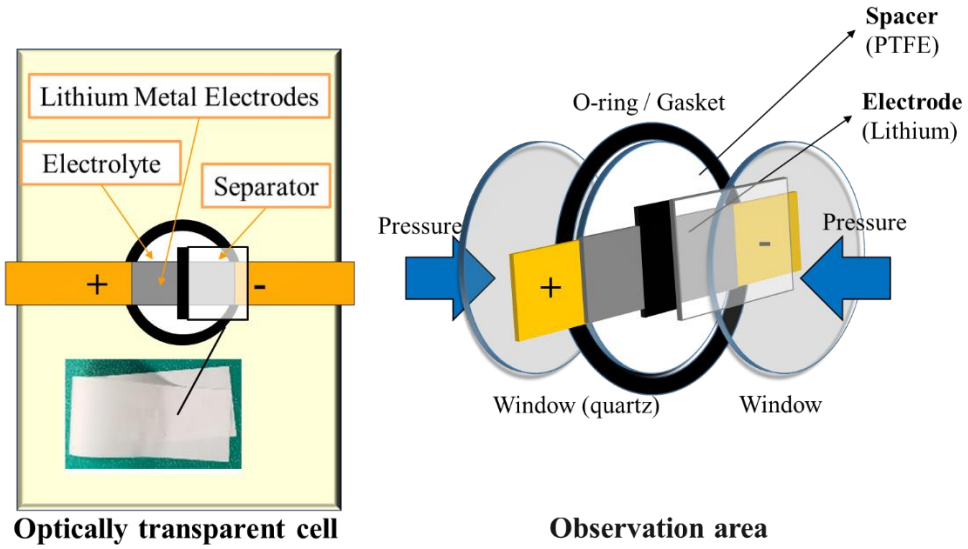

Figure 3.5 The implementation of a piece of separator onto the negative electrode.

3.4 Electrolytes

One of the two electrolytes is 1M $LiPF_6$ in EC: DMC (V: V, 50: 50) (Electrolyte A), with no additives. The other electrolyte is 1.20M $LiPF_6$ in EC/PC/EMC=20/10/70 (V/V/V) 90.5wt% with additives that count for the other 9.5 wt% of the electrolyte, including VC 1.5wt% + FEC 3wt% + PS 2wt% + PST 1wt% + LiDFOB 1wt% + SN 1wt% (Electrolyte B). The additives can facilitate the SEI formation process and thus suppress the lithium dendrite growth. For the convenience of further discussion, the first electrolyte will be named “electrolyte A,” and the second electrolyte will be designated as “electrolyte B.” The tests were conducted at room temperature.

3.5 Electrode

The electrode is made of lithium metal which sits on a copper foil. The pieces of lithium metal will be sealed within the O-ring to prevent air contamination, and the copper foil will work as the current collector to contact with the battery tester. The lithium metal is from Aldrich and has a thickness of 0.38 mm. Electrode fabrication and assembly were conducted inside a glovebox with ultra-high purity Argon gas. Before the assembly, the surface layer of the lithium foil and copper was removed by sandpaper to remove the oxidation layers. Then, the lithium foil is rolled on copper foil (also from Aldrich, with a thickness of 25 μm and a width of 5 mm).

3.6 Separator

The separator is Entek® Gold LP UHMWPE (ultrahigh molecular weight polyethylene). The property of the separator is listed here [75].

Table 3.1 Separator properties

Material	Thickness, μm	Porosity, %	Gurley, s 100 cm^{-3} (JIS)	Puncture strength, g
UHMWPE	19.4	37	394	432

3.7 Post-mortem examination procedure of the separator

The sample was disassembled inside the glovebox after the dendrite growth test. After the disassembly, some of the formed dendrites are attached to the separator. The attached dendrite and the separator were transferred into the SEM for morphology analysis. After the SEM examination, the dendrite and separator were immersed in water to remove the lithium dendrite without causing mechanical deformation of the separator. Thus, the protrusion left on the separator preserves the shape of the dendrite underneath the separator. To closely examine the protrusion area on the separator, 6nm metal coating layers of Au-Pd (60/40) were applied on both sides of the separator. With the coating layer, the separator was examined under SEM. Figure 3.6 shows the relationship among the images collected at various stages.

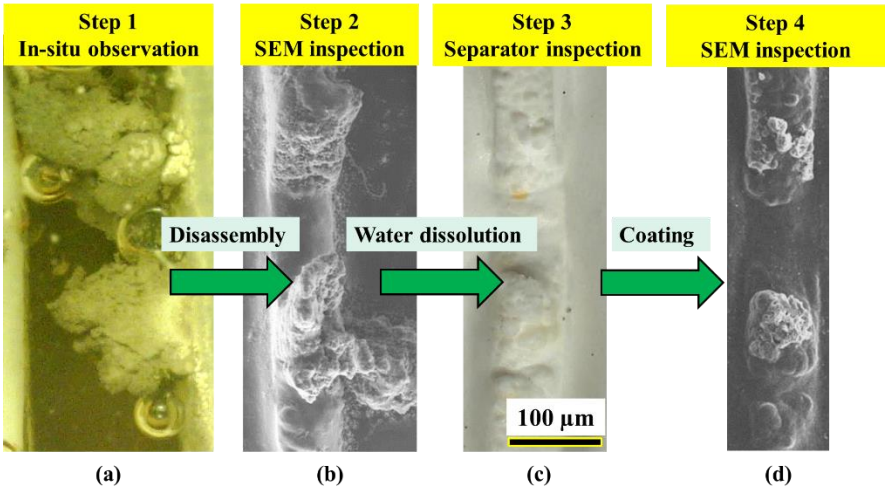

Figure 3.6 Visual inspection steps: (a) optical image of separator and dendrite collected during the test, (b) SEM image of separator with dendrite taken after the test, (c) protrusion left on the separator caused by dendrite growth, and (d) SEM image of the protrusion area on the separator after metal layer coating.

3.8 Determination of the limiting current density

Since the lithium dendrite growth is related to the mass transport of the lithium ions, the electrolyte limiting current density was estimated from the linear sweep voltammetry (LSV) before conducting the dendrite growth test. Figure 3.7 shows the LSV results scanned at 1 mV/s until 3V. The current was converted into current density based on the initial cross-sectional area of the negative electrode at the beginning of the test. Since the lithium dendrite was formed during the LSV test, which can inevitably increase the surface area, the current density can be lower than the value determined here. Fortunately, the limiting current density was determined when the curve shows the plateau that indicates the cell reaches the mass transport limit. The surface area is less affected by the dendrite growth at this moment. From the measurement, the limiting current density for electrolyte A is about 100 mA/cm^2. The limiting current density for electrolyte B is about 10 mA/cm^2.

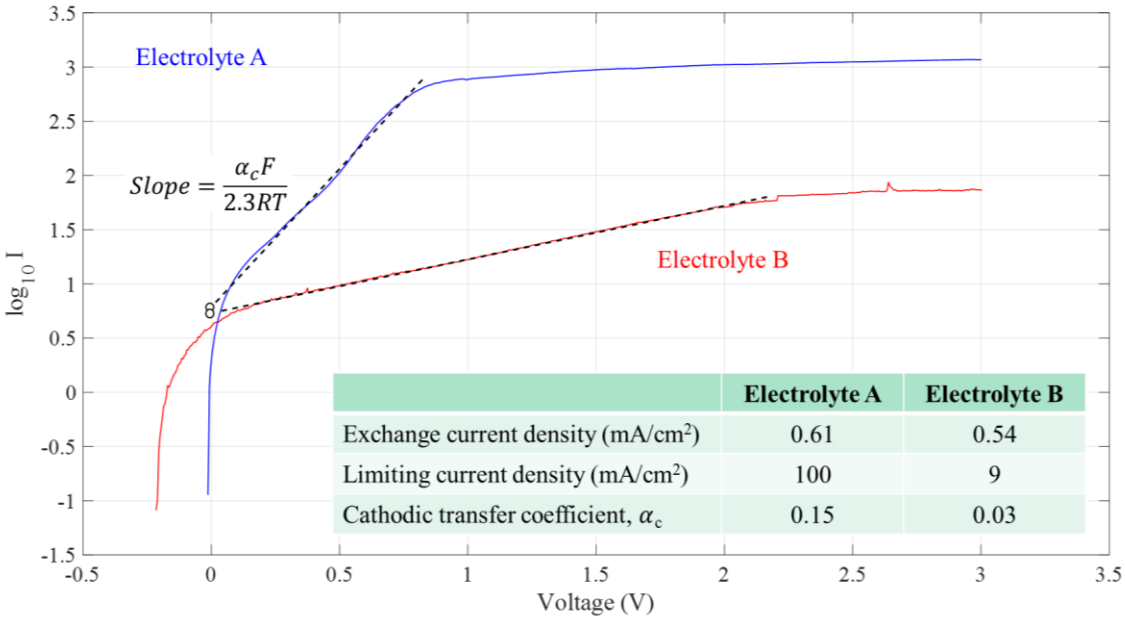

	Electrolyte A	Electrolyte B
Exchange current density (mA/cm^2)	0.61	0.54
Limiting current density (mA/cm^2)	100	9
Cathodic transfer coefficient, α_c	0.15	0.03

Figure 3.7 The LSV results for two electrolytes.

3.9 Design of experiments for in-situ lithium dendrite growth

To determine the influence of electrolyte, initial current density, and separator on the lithium dendrite growth, the constant current tests were conducted based on the conditions listed in Table 3.2.

Table 3.2 Design of experiments for in-situ lithium dendrite growth

Electrolyte	**Initial Current Density (mA/cm^2)**	**No Separator**	**Separator Implemented**
Electrolyte A 1M $LiPF_6$, EC: DMC (1:1, V:V)	1	×	
	5	×	
	10	×	×
	20	×	
	30	×	
	40	×	
	50	×	
	87	×	
	95	×	
	110	×	
	125	×	
Electrolyte B 1.20M $LiPF_6$, EC/PC/EMC=2/1/7(V:V) 90.5wt% + VC 1.5wt% + FEC 3wt% + PS 2wt% + PST 1wt% + LiDFOB 1wt % + SN 1wt%	10	×	×
	20	×	
	30	×	×

Chapter 4: Influence of Current Density on Lithium Dendrite (Electrolyte A, without separator)

Galvanostatic tests were conducted under an ambient condition (around 25 °C) at current densities ranging from 10 to 125 mA/cm^2, using an Arbin battery tester. The current densities were calculated based on the applied current and the electrode cross-section area. The optical images were collected using a digital microscope, and voltage/current signals were continuously recorded. ImageJ software was used to analyze optical images and measure the lithium dendrites' length changes. No separator was implemented at this step. This chapter incorporates the previously published journal article "In-situ observations of lithium dendrite growth [76]."

4.1 Results of dendrite growth under constant current

The dendrite growth tests were conducted under various current densities. The real-time dendrite images and the corresponding electrical signals were collected during the constant current charging process until an internal short circuit occurred. Since the dendrite growth is under mixed control in the lower current densities, the tests were repeated. Figure 4.1 shows the typical behavior of the lithium dendrite under different current densities, and the time indicates the time to the occurrence of dendrite-caused ISC. Some samples were explained in detail in the following sections.

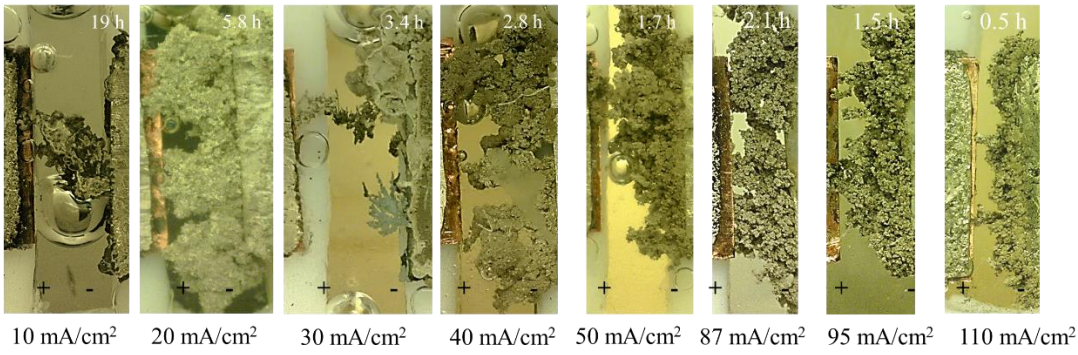

Figure 4.1 The evolution of the dendrite under different current densities. These images were taken at the moment the dendrite caused ISC.

Figure 4.2 shows the dendrite that formed on the upper part of the negative electrode when the initial average current density was 10 mA/cm^2. The local electrical field is likely to bias the lithium dendrite initiation position. In this case, a right-angle corner is a preferential spot due to its higher electric field intensity. The electric field was concentrated around the dendrite tips because of their higher aspect ratio. The first formed lithium dendrite changed the negative electrode's geometry and electrical field distribution. Thus, the dendrite tips have higher electrical field intensity than the rest of the flat electrode, and dendrite growth was enhanced at the preferential spot in the following charging process.

The sharp voltage drop at 7.3 h in Figure 4.2 indicates an internal short circuit. At the same time, the grown dendrite filled the gap between the positive and negative electrodes and connected them. The voltage recovered 0.3 h later to 0.1 V. A similar voltage recovery phenomenon was reported by Dollé et al. [77]. They observed a burnt mark in their sample, which they proposed was caused by the thermo-fusible effect, in

which the voltage recovery was attributed to the current-caused dendrite tip damage. This theory regarded the dendrite connecting two electrodes as a fuse. Once the two electrodes were connected, the current could go through the connecting point and cause a temperature rise that breaks the connection. The voltage recovery lasted about 1 h. However, under the constant current charging condition, the lithium dendrite kept growing toward the positive electrode and connected two electrodes again at 8 h, which made the voltage drop to zero. As shown by the dendrite images at 7.3 h and 9 h, the shape of the formed dendrite did not change for about 2 h. The dendrite growth stopped after the internal short circuit. The solid connection between the two electrodes was established, and the voltage remained stable after the second voltage drop (at 8.1 h).

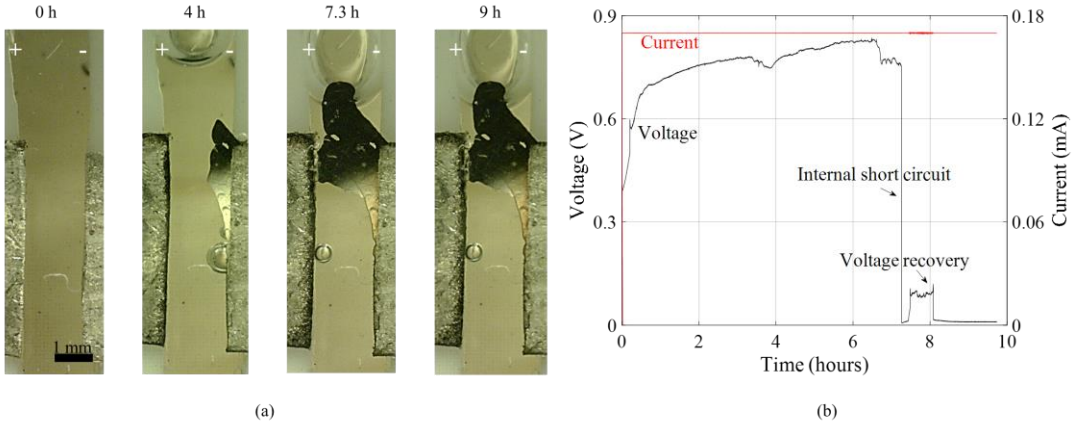

Figure 4.2 The evolution of the dendrite and the electrical signals at a current density of 10 mA/cm^2, (a) the optical images; (b) the corresponding voltage and current profile.

The lithium dendrite grew in the transverse direction as well as toward the positive electrode when the applied current density was 40 mA/cm^2. As shown in Figure 4.3, at

0.5 h, dendrites initiated mainly at three different spots (circled in Figure 4.3a) along the edge of the negative electrode. There was no significant dendrite growth between the two adjacent spots. After 2 h, lithium dendrites spread along the edge of the negative electrode, and the lithium dendrites at the initiation spots are longer. An internal short occurred at 3.8 h with a voltage drop. However, the voltage did not drop to zero. This phenomenon is called a "soft internal short" because the dendrite structure at such a high current density appears to be a cluster of big lithium particles, and loosely structured lithium dendrites are fragile and easy to break. Thus, in this situation, the voltage recovery may be a result of mechanical stress as well as the above-mentioned heating effect.

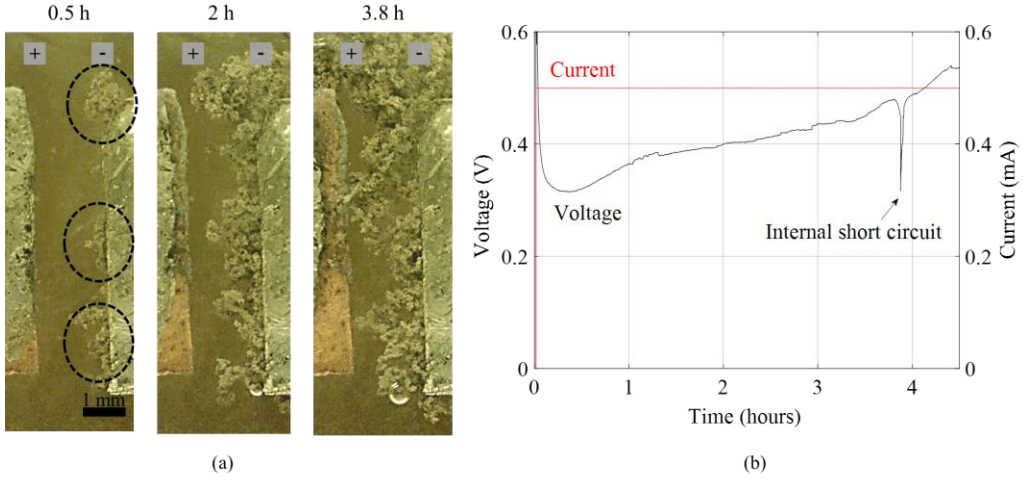

Figure 4.3 The evolution of the dendrite and the electrical signals at a current density of 40 mA/cm^2, (a) the optical images; (b) the corresponding voltage and current profile.

Figure 4.4 shows dendrite growth at 87 mA/cm^2. The dendrites initiated at the electrode corners are similar to the tests at 10 mA/cm^2. After 1 h, the dendrites gradually extended to the middle part of the electrode. Based on continuous observation, the dendrites in the middle are the extension of the dendrites initiated at the corners. However, the growth rate of the dendrites in the middle is lower than those at the corners. Although it seems the dendrite already connected the two electrodes at 1 h, the corresponding voltage data in Figure 4.4 shows the voltage drop occurred at 2.1 h. This time variation is due to the fact that the dendrites did not grow in the same plane. It is possible that the positive electrode and the dendrite tips in the image at 1 h were located in two different planes and seemed overlapped when the image was taken. The actual connection was built up at 2.1 h and caused the internal short circuit before the electrode connection; the voltage was stabilized around 0.6 V from 0.5 to 2.1 h, as shown in the voltage curve. At 2.1 h, due to the dendrite-caused internal short circuit, the current carrier changed from ions in the electrolyte to electrons in the metallic dendrite structure. The resistance of the metal is much lower than the conductive electrolyte, and the switching causes the voltage to drop sharply. If only the cell voltage is monitored, but the dendrite images are not available, there will be no significant sign of dendrite growth until the sharp voltage drop in the voltage data.

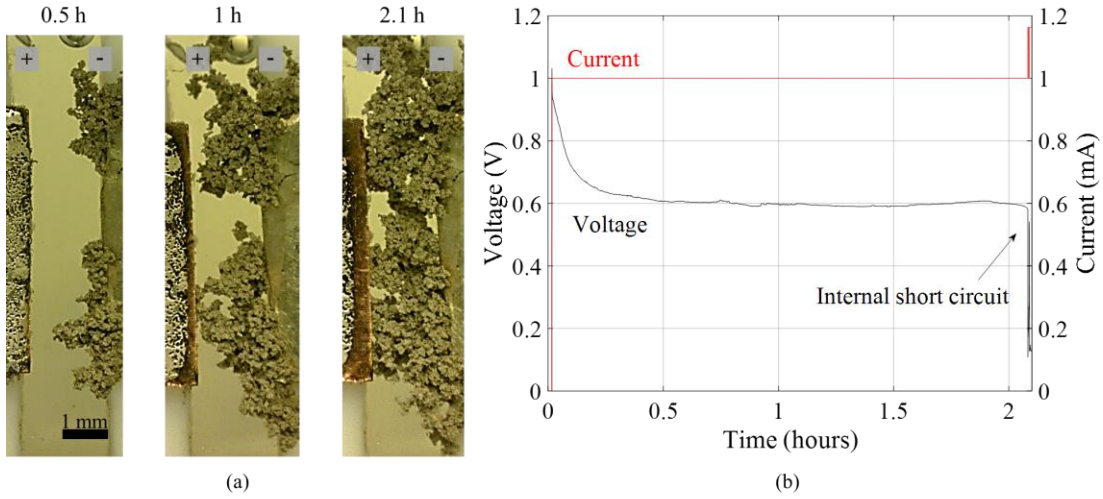

Figure 4.4 The evolution of the dendrite and the electrical signals at a current density of 87 mA/cm^2, (a) the optical images; (b) the corresponding voltage and current profile.

Figure 4.5 shows the dendrite growth at 95 mA/cm^2. At 0.5 h, the initial dendrites formed and covered the electrode edge, as shown in Figure 4.5(a). In this test, the initial dendrites along the edge were not formed at the same time. The initial lithium dendrite had a slightly different length due to the growth time variation. The dendrites initiated earlier are longer and have a higher aspect ratio than the rest. As mentioned in the previous tests, these longer dendrites were the favorable growth spots in the following charging process because the electrical field intensity was higher around them. The earlier growth retained the geometrical advantage. At 1.5 h, several needle-like dendrites presented and grew faster than the other flatly deposited lithium. This result is consistent with Brissot et al.'s paper [19], where the formed lithium dendrite grew at several points and had needle-like morphology. These needle-like dendrites led to the

first internal shorts. The voltage curve had a drop at 1.5 h, indicating the occurrence of an internal short circuit. At 1.5 h, there was a transient increase in the current data. This phenomenon further validates our understanding of the soft internal shorts, which usually do not last long. Therefore, although the voltage recovered, the first voltage drop should be regarded as a warning sign of an internal short circuit.

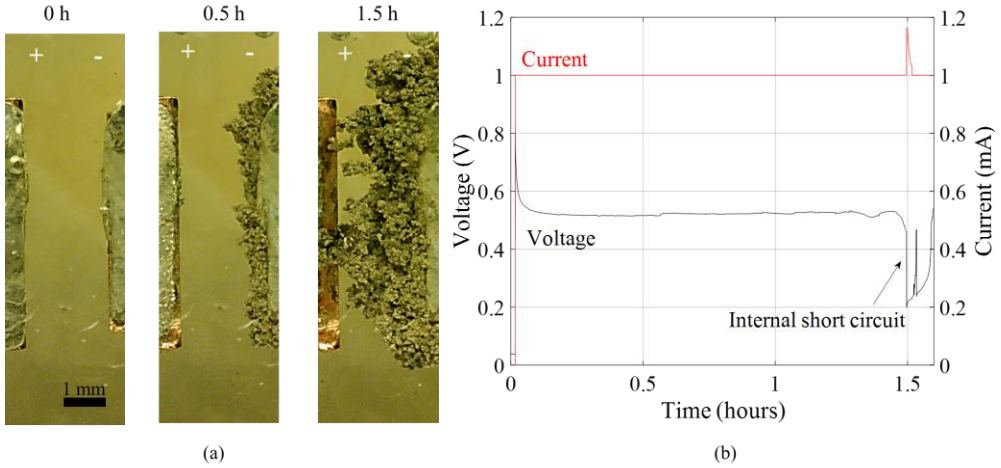

Figure 4.5 The evolution of the dendrite and the electrical signals at a current density of 95 mA/cm^2, (a) the optical images; (b) the corresponding voltage and current profile.

In Figure 4.6, the dendrites changed from the mossy growth into the needle-like form when charged at 110 mA/cm^2. Initially, the dendrite was deposited all along the electrode edge. Around 30 min, two needle-like dendrites connected the two electrodes, which was confirmed by the voltage curve. The formation of the needle-like structures hastened the internal short circuit process.

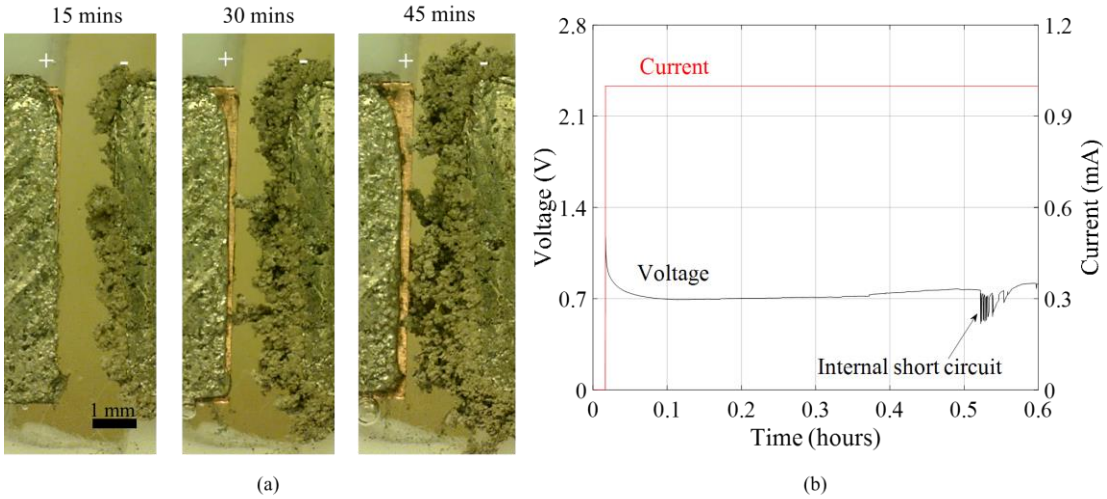

Figure 4.6 The evolution of the dendrite and the electrical signals at a current density of 110 mA/cm^2, (a) the optical images; (b) the corresponding voltage and current profile.

Test observations conducted at 125 mA/cm^2 are shown in Figure 4.7. The dendrite initiated at the electrode corners and the middle, which indicates the electrical field intensity at the middle part of the electrode is now comparable with that at the electrode corner, and the electrode geometry influence is weaker than in the previous tests. The cell voltage kept increasing from the start of the test, which is due to cell polarization. Charging at 125 mA/cm^2, the ion movement in the electrolyte reaches its maximum limitation, but the mass transfer in the electrolyte is lower than the charge transfer on the electrode. In other words, the mass transfer step is now the controlling step and limits the total reaction speed. The accumulated charges on the electrodes prevented the voltage from stabilizing around a specific value but increased, which was different from the voltage data in previous tests.

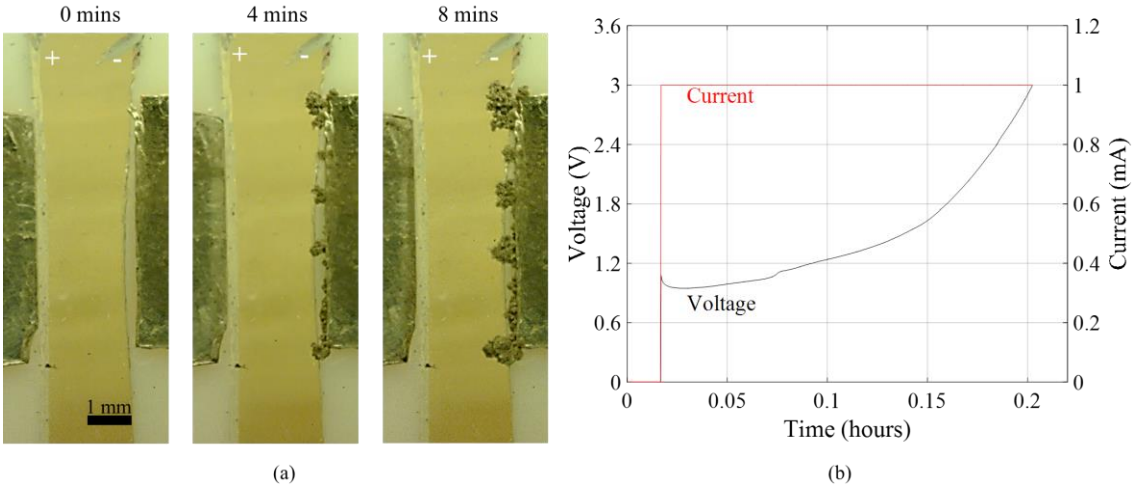

Figure 4.7 The evolution of the dendrite and the electrical signals at a current density of 125 mA/cm^2, (a) the optical images; (b) the corresponding voltage and current profile.

Once beyond the limiting current density, the higher current density will not increase the dendrite growth reaction but only the voltage. The increasing tendency of the voltage data shown in Figure 4.7 proved this and indicates that 125 mA/cm^2 is already beyond the limiting current density. In that test, the voltage increased higher than the upper limit (3.0 V) after only 12 min, and the test was stopped. In consideration of the LSV test result and the 125 mA/cm^2 test result, one reasonable estimation of the limiting current density for EC: DMC 1 M $LiPF_6$ electrolyte is in the range of 100 to 125 mA/cm^2.

4.2 Analysis of dendrite growth at various initial current densities

The sharp voltage drop indicated an internal short circuit, which was cross-checked with the dendrite images. The time to the first voltage was considered as the elapsed time before the internal short circuit. The growth rate of the dendrites under different current densities was calculated by dividing the dendrite length by the elapsed time until the first voltage drops to evaluate the average dendrite growth rate under certain current densities (see Table 4.1). In Table 4.1, the initial current density is the average current density calculated at the beginning of the test. The tests under 10, 30, 40, and 50 mA/cm^2 were repeated several times.

Table 4.1 Time to First Voltage Drop and Growth Rate

Current Density (mA/cm^2)	**Plateau voltage (V)**	**Time to ISC (hrs.)**	**Average growth rate (mm/h)**
10	0.8	7.3	0.2
10	0.3	3.8	0.7
10	1.0	19.0	0.1
20	0.2	5.8	0.4
30	0.8	4.1	0.6
30	0.8	3.4	0.9
30	0.4	2.6	0.8
40	0.3	3.9	0.4
40	0.8	2.8	1.0
40	0.5	3.4	0.6
50	0.7	1.9	1.1
50	0.6	1.7	1.2

87	0.6	2.1	0.9
95	0.5	1.5	1.7
110	0.7	0.5	2.2
125	1.0	N/A	5.0

The dendrites that grew under different current densities have different growth rates and morphologies. The times when the dendrite length was equivalent to half of the gap between the two electrodes are summarized in Table 4.2. Based on the time to half of the gap, the estimated times to the first voltage drop are compared with the actual times to the first voltage drop. The results are plotted in Figure 4.8. At 10 and 100 mA/cm^2, the estimated values match the actual ones. However, in the middle part, the estimated times are faster than the actual ones owing to the different growth processes. At 10 and 110 mA/cm^2, the dendrites grew in the same morphology from the start of the test until the end. They all grew directly toward the positive electrode, but when the current density was in the middle range, they grew in the transverse direction.

Table 4.2 Time to First Voltage Drop and Growth Rate

Initial current density (mA/cm^2)	Time to half of the gap (h)	Time to first voltage drop (h)	Growth rate (mm/h)	Cell voltage (V)
10	3.7	7.3	0.23	0.8
40	0.45	3.88	0.43	0.3
87	0.35	2.08	0.92	0.6
95	0.53	1.48	1.7	0.5

110	0.23	0.5	2.18	0.7
125	N/A	N/A	4.96	1.0

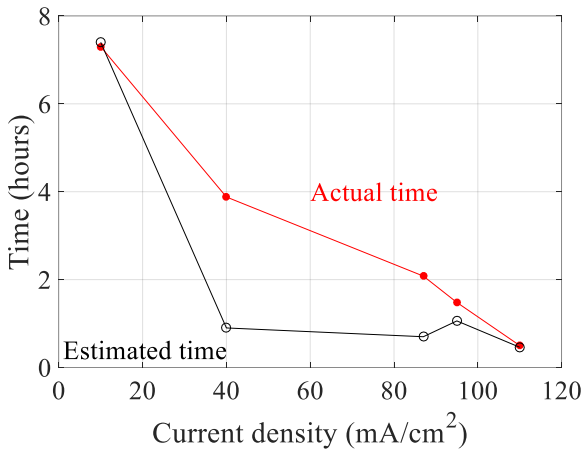

Figure 4.8 Comparison between the estimated time and the actual time to the first voltage drop.

The growth rates are plotted against the current densities in Figure 4.9. As expected, with the increase in current density, the time to the first voltage drop decreases. The internal short circuit process is hastened with the increased current densities, which is due to the dendrite morphologies change. The needle-like structures shown at higher current densities have a higher aspect ratio than the mossy dendrite and can connect the two electrodes in a shorter time.

After 95 mA/cm^2, the dendrite growth rate is not only higher than the previous test results, but the curve slope is also steeper. This is due to the change in dendrite morphologies, as previously discussed. Previously, the dendrites initiated at the corners of the negative electrode and extended in the transverse direction as well as grew toward the positive electrode. However, with the increase in current density, the dendrite that initiated along the electrode edge and gradually switched to a needle-like structure grew toward the positive electrode directly. In the test at 125 mA/cm^2, the initiated dendrite was already in the needle-like form.

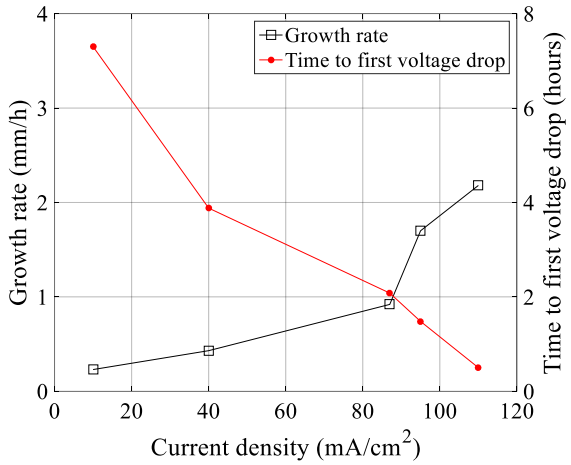

Figure 4.9 Time to first voltage drop and growth rate under various current densities.

4.3 Generic functional equation for dendrite growth

The test results shown in Table 4.1 include multiple repeated test results from various initial current densities. To obtain a generic functional equation to describe the lithium dendrite growth in electrolyte A, the averaged values of the average dendrite growth rate for the repeated results were used in the curve fitting. The standard error (eq. 4.2)

for the test results under 10, 30, 40, and 50 mA/cm^2 were calculated based on the mean values. Since only one data point was available for the rest of the conditions, the error was not calculated. The mean, standard deviation, and standard error were summarized in Table 4.3.

$$standard\ deviation\ \sigma = \sqrt{\frac{\sum_{i=1}^{n}(x_i - \bar{x})^2}{n-1}} \quad \text{(eq. 4.1)}$$

$$\bar{x} = the\ sample's\ mean$$

$$n = the\ sample\ size$$

$$standard\ error\ (\sigma_{\bar{x}}) = \frac{\sigma}{\sqrt{n}} \quad \text{(eq. 4.2)}$$

Table 4.3 Standard error of mean

Initial current density (mA/cm^2)	**Mean of average growth rate (mm/h)**	**Standard deviation of average growth rate (mm/h)**	**Standard error of mean**
10	0.33	0.32	0.19
30	0.77	0.15	0.09
40	0.67	0.31	0.18
50	1.15	0.07	0.05

Figure 4.10 shows the dendrite growth rate under various initial current densities of 10-125 mA/cm^2. And the fitting result is shown in Figure 4.11. The parameters (A and B) for the generic function equations are listed in Figure 4.11. The fitting accuracy R^2

value (0.89) was calculated based on either the single data or the means of repeated tests.

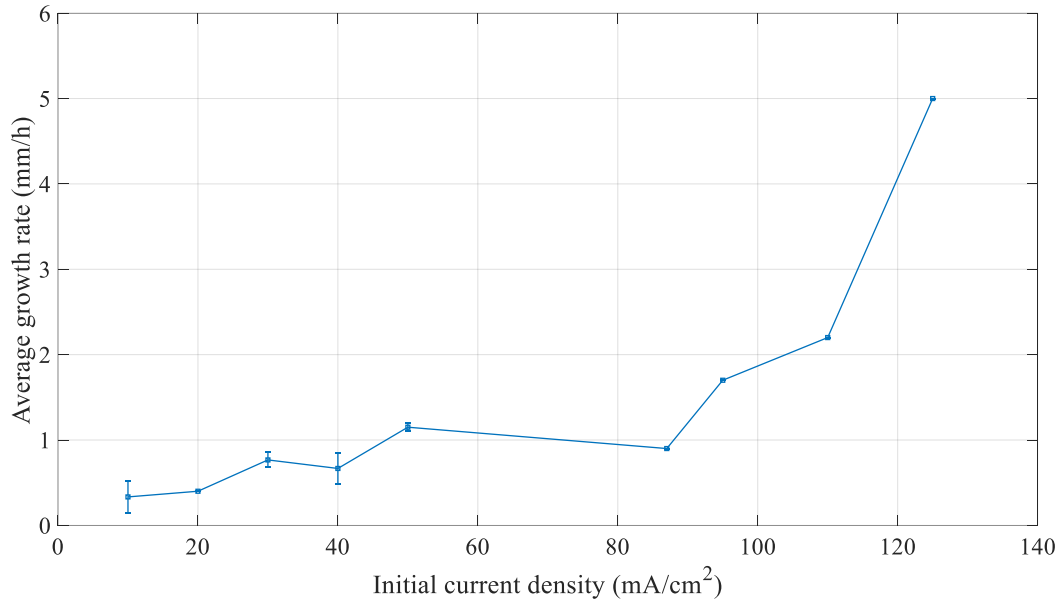

Figure 4.10 Dendrite growth rate under various initial current densities 10-125 mA/cm^2.

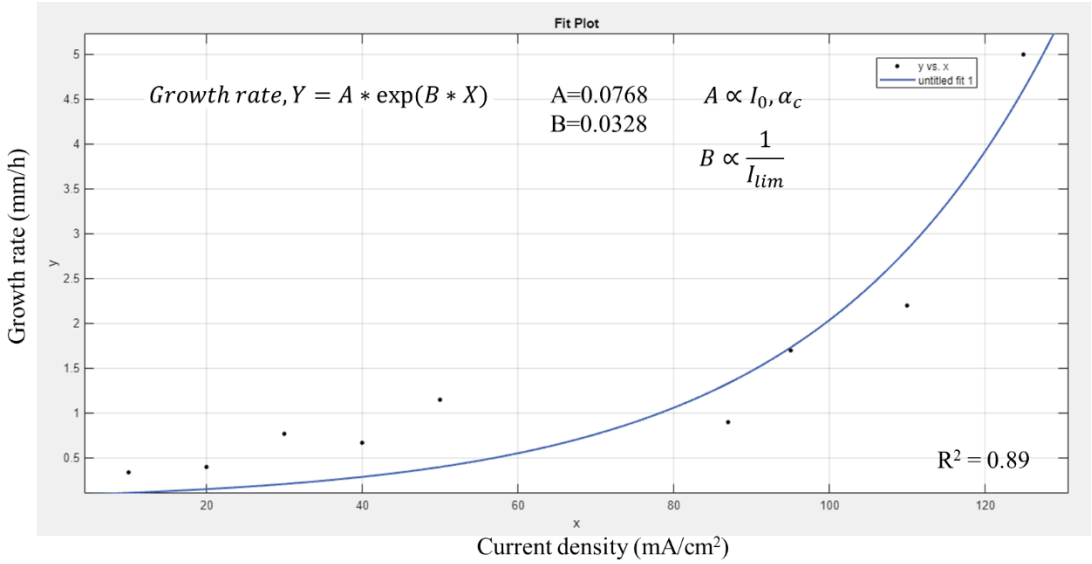

Figure 4.11 Generic functional equation for dendrite growth in the electrolyte a.

4.4 Observation of lithium dendrite microstructure

Figure 4.12 is the dendrite formed after the test. Since the negative electrode is located on the right-hand side. The dendrite near the right is the dendrite formed in the early stage. Multiple rings can be seen on the lithium dendrite, which was formed due to the growing spot alternation.

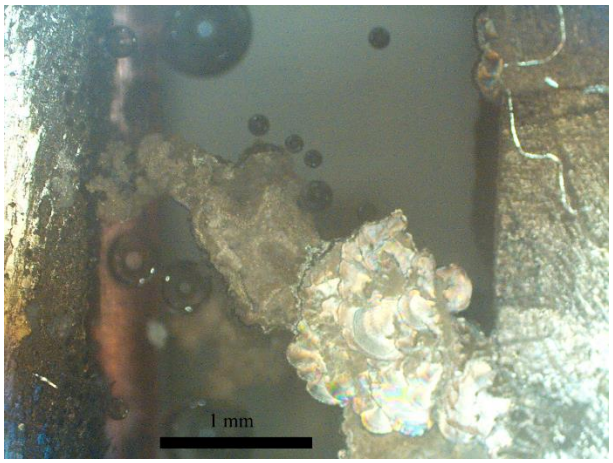

Figure 4.12 The optical image of the dendrite formed under 10mA/cm^2.

In addition, the transition of the dendrite morphology was also observed in the sample under 20 mA/cm^2. Figure 4.13 shows the lithium dendrite formed in the early stage, and Figure 4.14 shows the lithium dendrite formed in the later stage. It can be seen that the dendrite changed from granular morphology into a short needle structure.

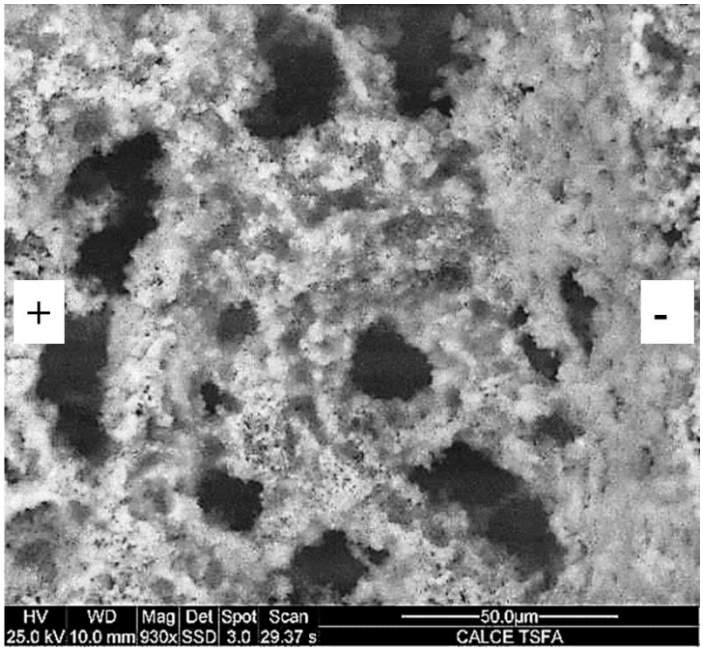

Figure 4.13 SEM image of the lithium dendrite (granular dendrite) from the early stage under 20 mA/cm^2. The signs in the image indicate the orientation.

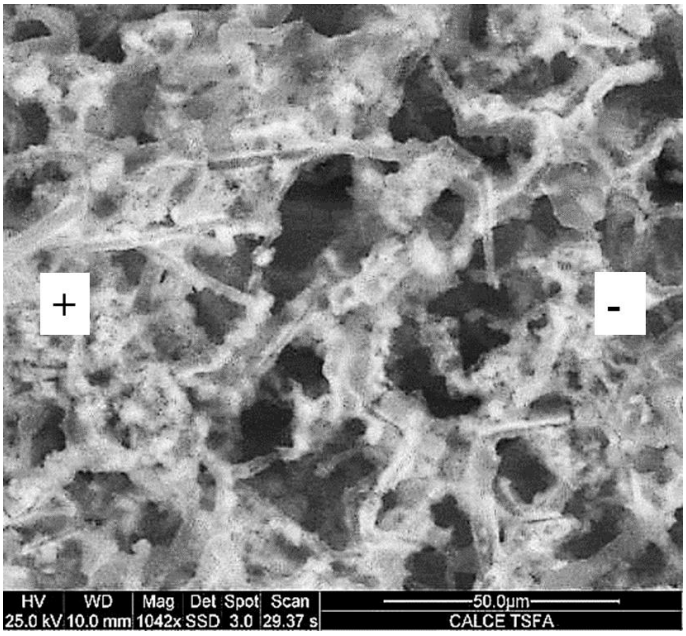

Figure 4.14 SEM image of the lithium dendrite ("short needle") from in the later stage under 20 mA/cm^2. The signs in the image indicate the orientation.

Chapter 5: Influence of Current Density on Lithium Dendrite (Electrolyte B, without separator)

The lithium dendrite growth tests in electrolyte B systems were conducted under three current densities: 10, 20, and 30 mA/cm^2. Constant current charging tests were conducted until the occurrence of dendrite triggered ISC.

5.1 Results of dendrite growth under constant current

Figure 5.1 is the cell voltage from the beginning of the tests until the dendrite triggered ISC. The insert image shows the voltage profile from the first 670s. In this section, the voltage jumped from almost 0 to a peak value due to the application of current, then the voltage gradually decreased. The peak voltage values in the first 670s are 0.42 V for 10 mA/cm^2, 0.83 V for 20 mA/cm^2, and 0.94 V for 30 mA/cm^2. Based on [78], the section between the voltage peak and the time the voltage reaches a plateau is related to the nucleation process. The following plateau section is the growth regime. For the test under 10 mA/cm^2, the voltage did not get stabilized in the first 12 hours. Combined with the voltage increases, continuous gas generation was observed after the voltage increased again and entered the region higher than 0.5 V. According to [79], the lithium dendrite will transit from base-controlled growth to tip-controlled growth. The base-controlled growth can lead to unstable in the SEI layer.

Figure 5.2 shows the dendrite growth process under three current densities. The last image in each column is the dendrite image captured when the ISC occurred. With the voltage increases, the dendrite growth rate is higher, but the efficiency is decreasing.

In addition, compared with the dendrite growth at higher current density (20 and 30 mA/cm^2), the dendrite growth at 10 mA/cm^2 switched from everywhere over the negative electrode to a localized region.

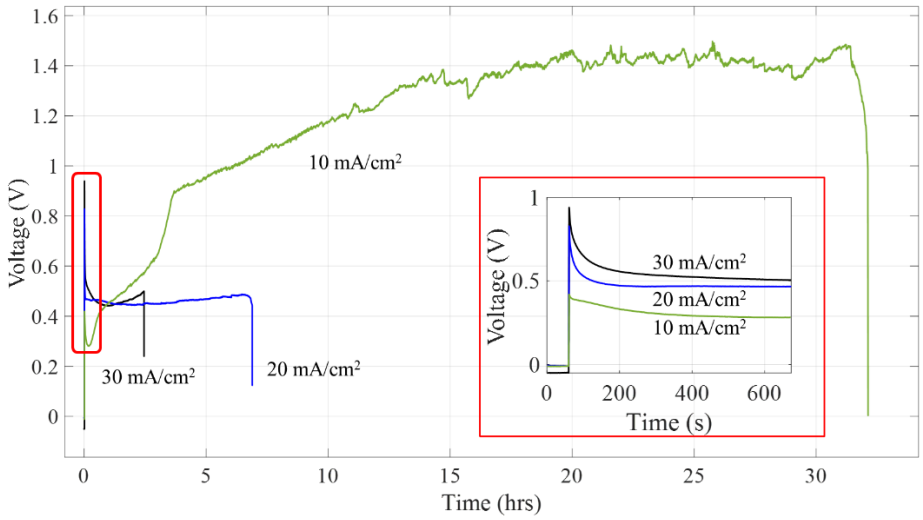

Figure 5.1 The voltage between the test start and the ISC occurrence. The insert image shows the voltage change in the first 670s.

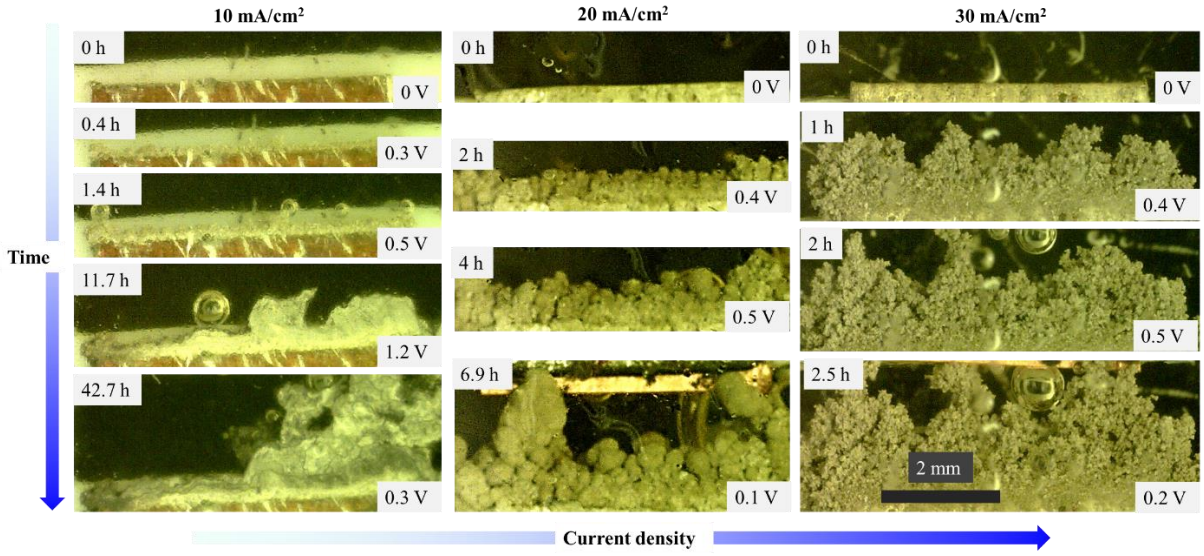

Figure 5.2 In electrolyte B, lithium dendrite growth process under 10, 20, and 30 mA/cm^2.

5.2 Analysis of dendrite growth at various initial current densities

Table 5.1 Summary of the lithium dendrite test results in electrolyte B

Cell No.	**1**	**2**	**3**
Current Density	10 mA/cm^2	20 mA/cm^2	30 mA/cm^2
Plateau voltage (V)	1.4	0.5	0.5
Time to ISC (hrs.)	32.0	6.9	2.4
Average growth rate (mm/h)	0.11	0.33	0.94
The charge transferred until ISC (C)	14.1*	9.7	5.0
Lithium dissolved from the positive electrode (C)	10.9	4.0	1.0
Efficiency	77.3%	41.0%	20%

*Due to the malfunction of the software, images between 23.3 hrs. and 42.7 hrs. were not captured. The measurement and calculation were conducted based on the data at 23.3 hrs.

The efficiency was calculated based on the following equation:

$$\theta = \frac{Q_1}{Q_2} = \frac{\Delta L * W * T * \rho * M * F}{Q_2} \quad \text{(eq. 5.1)}$$

Where ΔL is the change in the edge distance on the positive electrode, W is the width of the positive electrode, T is the thickness of the lithium foil on the positive electrode, ρ is the density of lithium metal, M is the molar mass of lithium, and F is the Faraday constant.

The test results shown in Table 5.1 include multiple repeated test results from various initial current densities. With the increase of the initial current density, the efficiency of the lithium deposition is decreasing. Two reactions lead to the lithium dissolving from the positive electrode. One is the lithium dissolved due to the electrochemical reactions to form lithium dendrite on the negative electrode; the other is the lithium consumed by the direct reaction between the lithium metal and the electrolyte. Figure 5.3 shows the EIS results from an assembly sample without experiencing any dendrite growth. However, the EIS evolved as time went by; this indicates the continuous reaction between the lithium metal and the electrolyte. Fresh lithium metal was kept exposed to electrolyte during the electrochemical reaction. Thus, there are chemical reactions between the lithium metal and electrolyte throughout the dendrite growth process. The electrolyte decomposition triggered by the lithium metal consists of multiple steps, and the electrolyte decomposition can be the reason that there is more charge consumed that is not contributing to the metal deposition process.

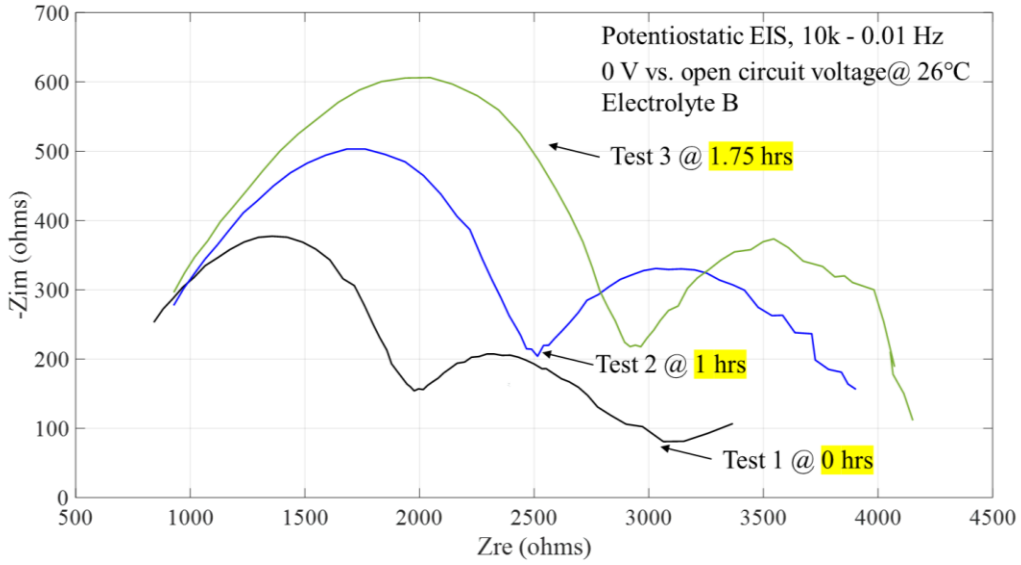

Figure 5.3 EIS evolution caused by the direction reaction between the lithium metal and electrolyte.

With the initial current density increase, the average dendrite growth rate increases. However, the transferred charge and the dissolved lithium decreased as the initial current density increased, and the dendrite reached the positive electrode with lower lithium deposition in a shorter time. This indicates that the dendrite formed at the higher initial current density has a porous structure, while the dendrite formed at the lower initial current density has a dense structure.

5.3 Generic functional equation for dendrite growth

The average dendrite growth rate under 10, 20, and 30 mA/cm^2 were used for curve fitting and determining the generic functional equation for dendrite growth in electrolyte B. Figure 5.4 shows the dendrite growth rate under various initial current

densities 10-30 mA/cm^2. And the fitting result is shown in Figure 5.5. The parameters (A and B) for the generic function equations are listed in Figure 5.5. The fitting accuracy R^2 value (0.99) was calculated based on the single data obtained under each initial current density.

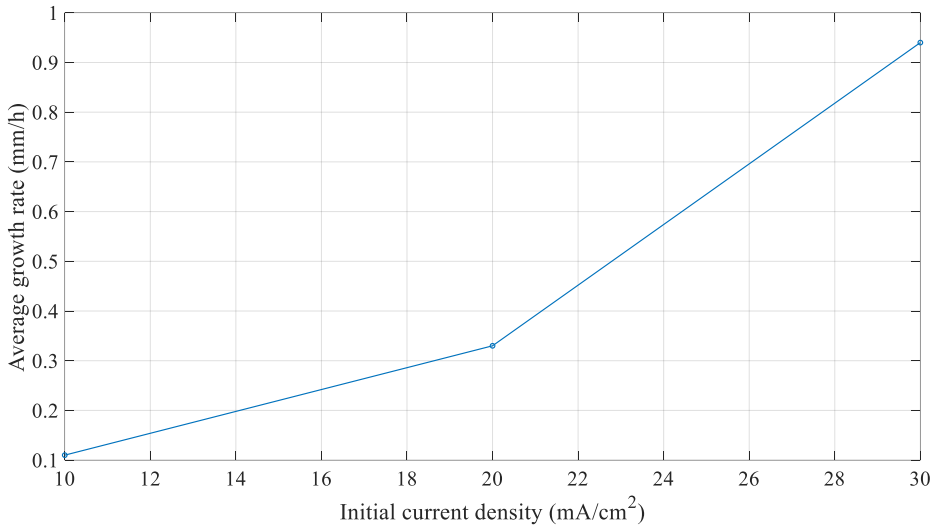

Figure 5.4 Dendrite growth rate under various initial current densities 10-30 mA/cm^2.

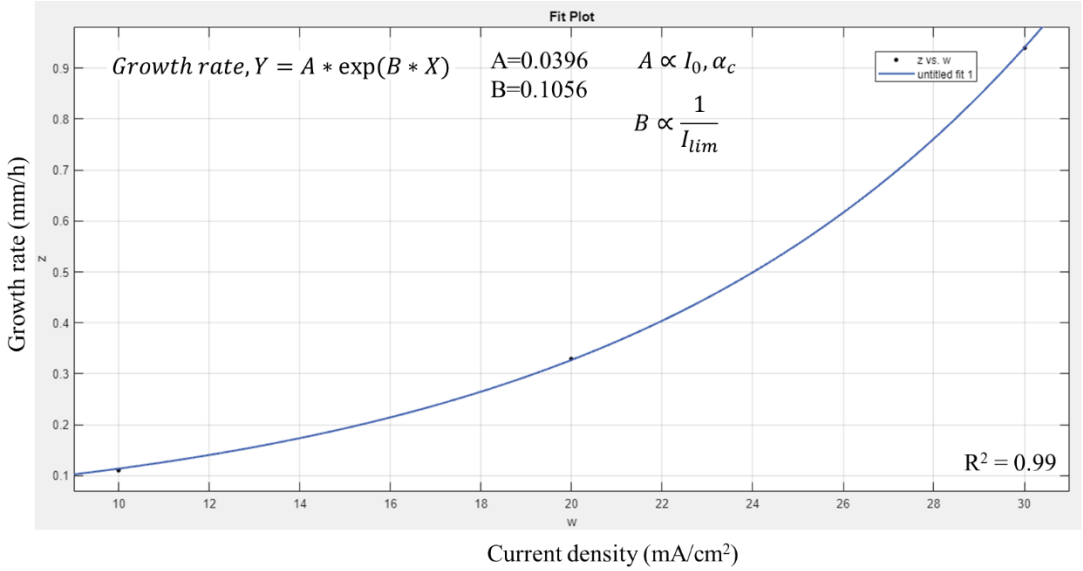

Figure 5.5 Generic functional equation for dendrite growth in electrolyte B.

5.4 Observation of lithium dendrite microstructure

The sample under 10mA/cm^2 was disassembled after the test, and the dendrite was observed by SEM. Figure 5.6 shows the lithium dendrite that has a granular morphology. This is the dominant morphology in this sample.

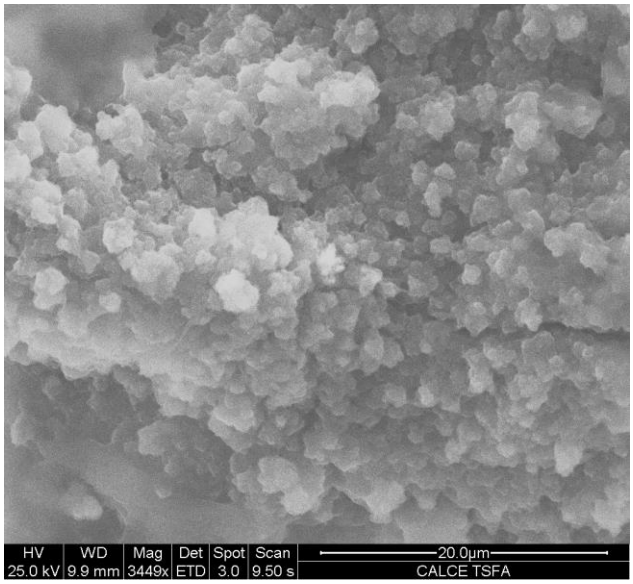

Figure 5.6 SEM image of the granular lithium dendrite formed under 10mA/cm^2 in electrolyte B.

Chapter 6: In-Situ Lithium Dendrite Growth with A Separator

In this section, dendrite growth tests were conducted with a separator implemented on the negative electrode in both electrolytes A and B. The applied current density was 10 mA/cm^2.

6.1 Dendrite growth with separator implemented in electrolyte A

Figure 6.1 shows the dendrite growth with a separator covering the negative electrode, sample 1, with electrolyte A. The dendrite initially grew at the upper corner and grew through the separator at around 2 hours. Figure 6.2 shows the separator retrieved from sample 1 after the test.

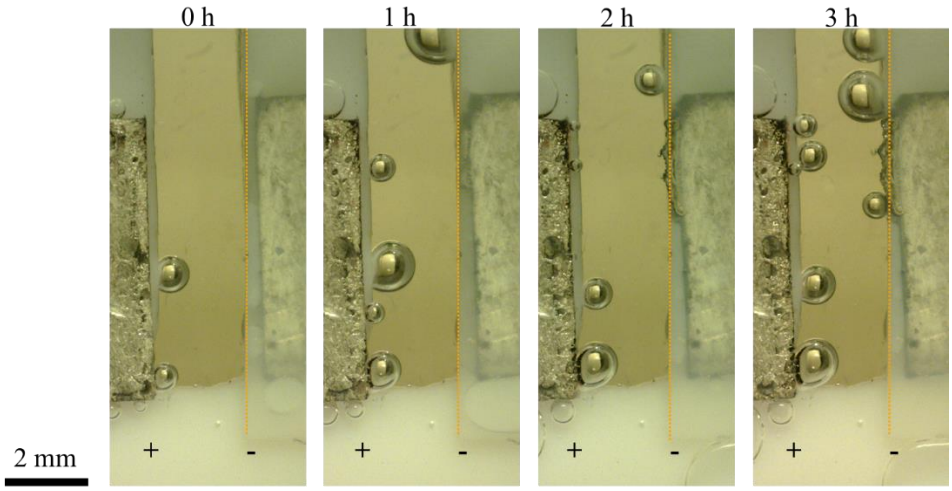

Figure 6.1 10mA/cm^2, sample 1 images.

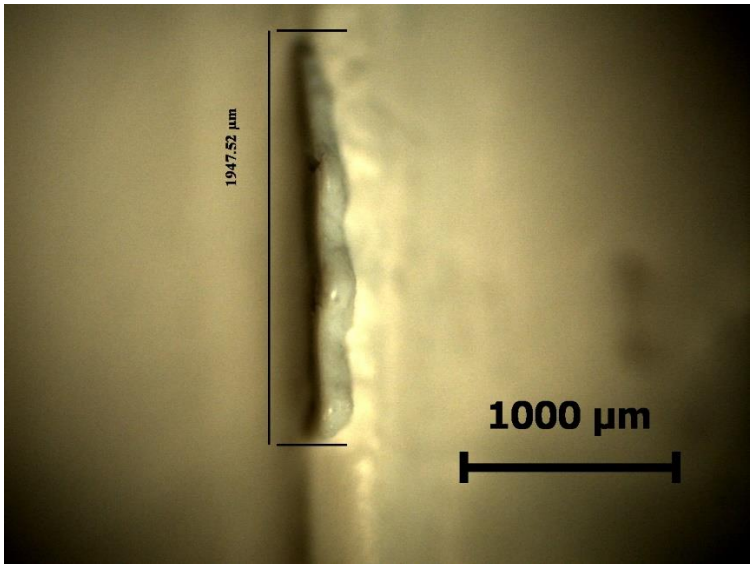

Figure 6.2 Separator from sample 1 after the test.

6.2 Dendrite growth with separator implemented in electrolyte B

From the dendrite growth tests conducted without a separator, it was shown that the dendrite formed under 10 mA/cm^2 has a dense structure compared to the dendrite formed at a higher current density (30mA/cm^2). Two lithium dendrite growth tests were conducted at 10 and 30 mA/cm^2 in electrolyte B. The dendrite formed under 10mA/cm^2 penetrated through the separator, while the dendrite formed under 30 mA/cm^2 was blocked. Their test results are shown below, and the sample 2 (10mA/cm^2) was further analyzed and the results were shown in section 6.3 (The SEM examination of the formed lithium dendrite and the separator).

Sample 2 (Figure 6.3) was tested under the initial current density of 10 mA/cm^2 with electrolyte B. The morphological evolution in the first 30 hours is shown in Figure 6.3. The images were taken at the beginning of the test (0 h), 10 h, 20 h, and 30 h. Close to

the bottom of the negative electrode formed the first dendrite, which grew beyond the folding edge of the separator at around 17 hours. Later, near the top of the negative electrode, the second growing spot formed where the dendrite grew beyond the separator.

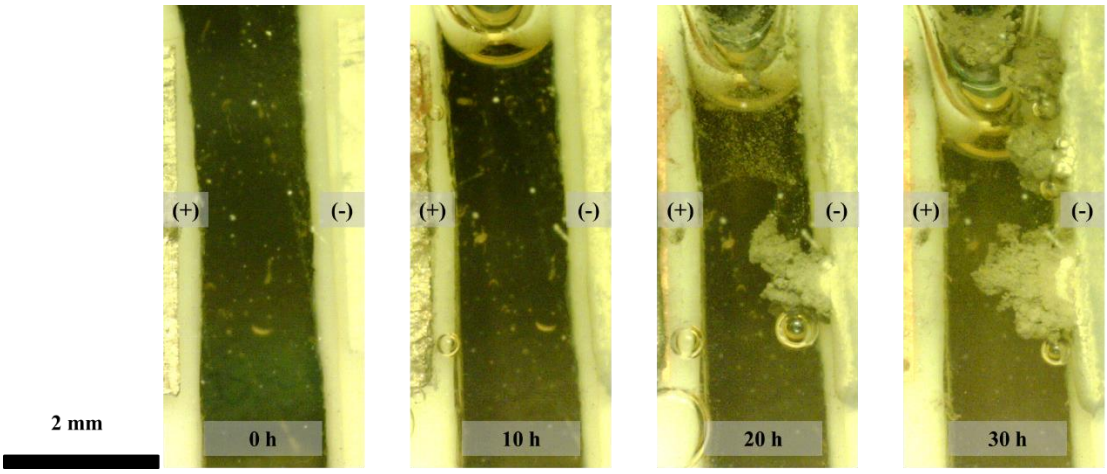

Figure 6.3 10mA/cm^2, sample 2, images at 0 h, 10 h, 20 h, and 30 h.

In the other test under 30mA/cm^2, the separator blocked the formed dendrite. Figure 6.4 shows the result. The lithium dendrite growth did not penetrate the separator applied on the negative electrode. Furthermore, the existence of the separator forced the dendrite to move upward.

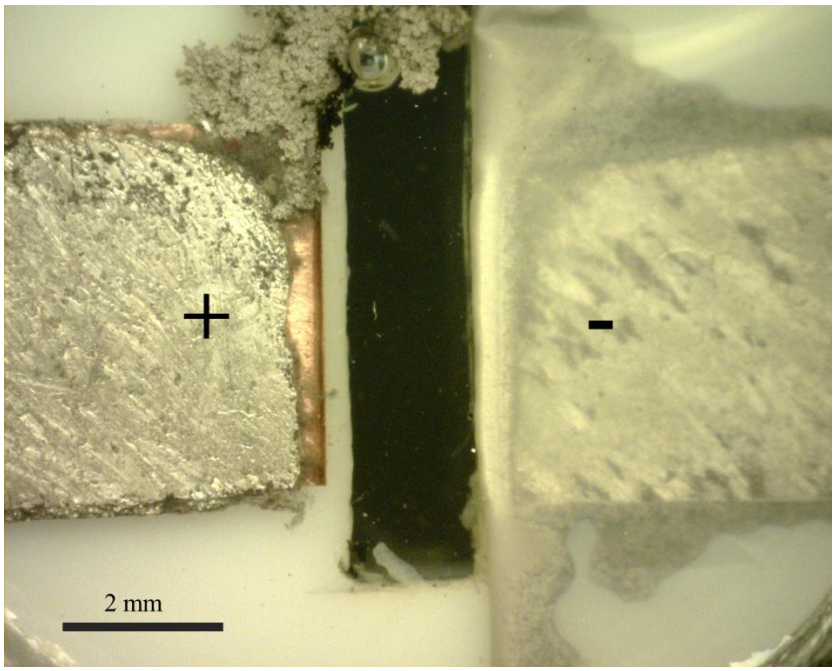

Figure 6.4 30mA/cm^2, sample 3, dendrite image at 9 h.

6.3 The SEM examination of the formed lithium dendrite and the separator

During the SEM examination, the dendrite formed after penetrating the separator was examined first. The dendrite near the second growing spot shows granular structures. The results are shown in Figure 6.5.

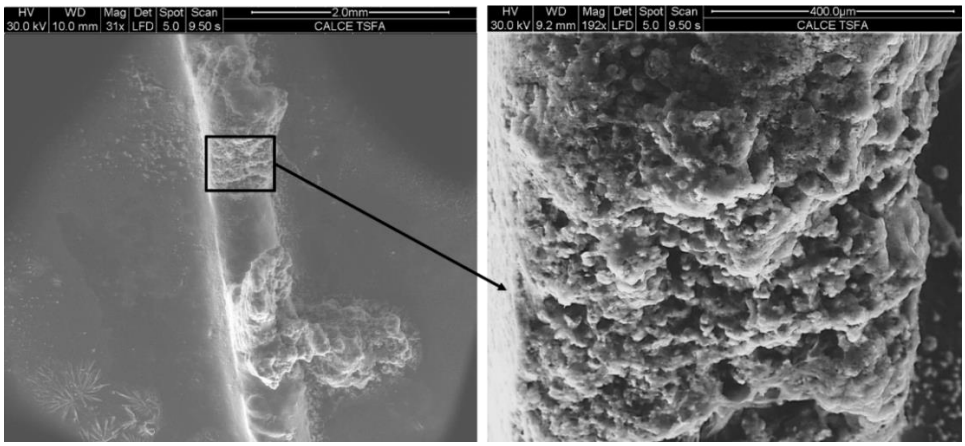

Figure 6.5 Granular dendrite on the section grew beyond the separator.

The separator was examined under optical microscopy and SEM after removing the dendrite. Due to the dendrite growth, the separator was significantly deformed at the interaction region (Figure 6.6), while the region not influenced by the dendrite growth still shows a flat surface morphology.

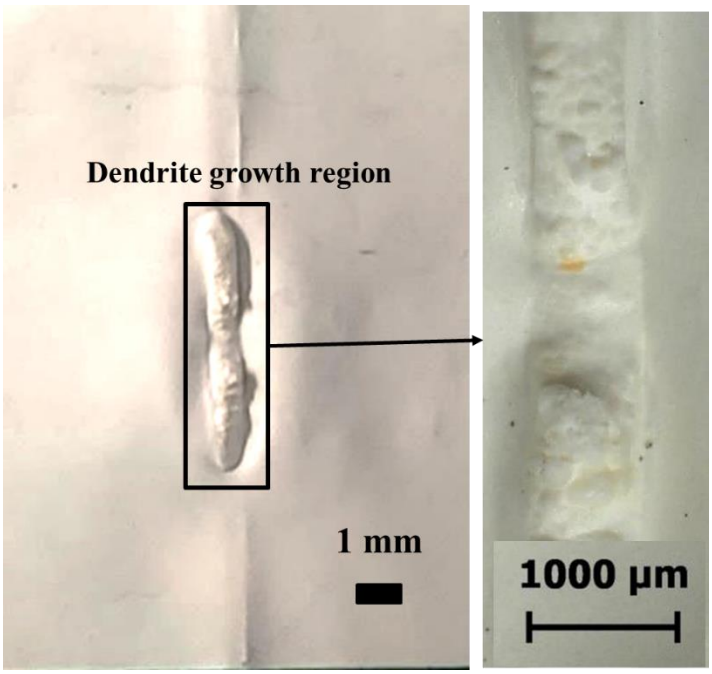

Figure 6.6 The separators after dendrite growth.

During the SEM examination of the dendrite-separator interaction area, two interaction modes between the separator and the dendrite were identified; the dendrite can either penetrate the separator or be blocked (Figure 6.7). Several pin holes were found at the dendrite penetration region. The sizes of the pin holes range from 14 to 26 µm, comparable to the separator's thickness (19 µm). Figure 6.7 shows the dendrite penetration region and the blocking region on the dendrite-separator interaction area. The surface morphology of the unaffected separator (Figure 6.8 left) and the dendrite penetrating area (Figure 6.8 right) were compared in Figure 6.8. The separator was torn,

and the straight white line in the image is the polymer separator stretched by the dendrite growth.

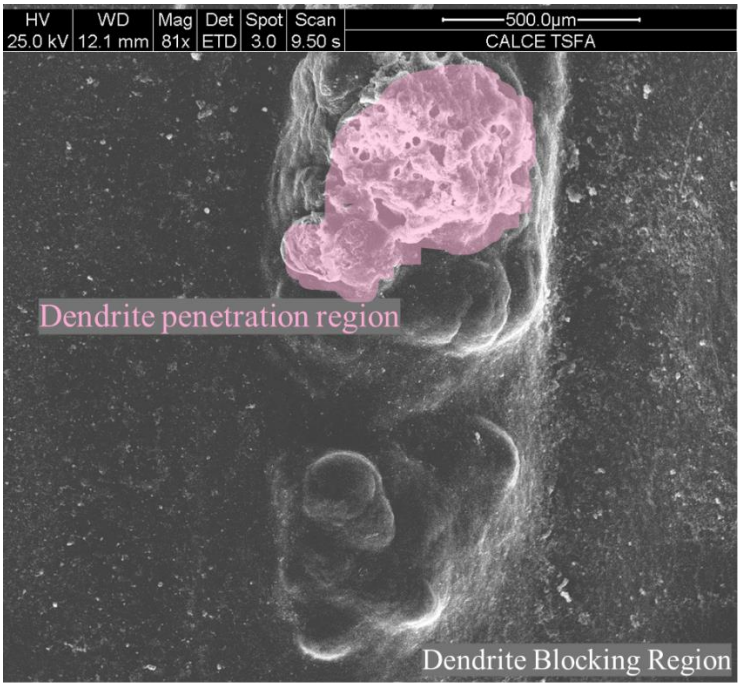

Figure 6.7 The dendrite penetration region and the blocking region on the dendrite-separator interaction area.

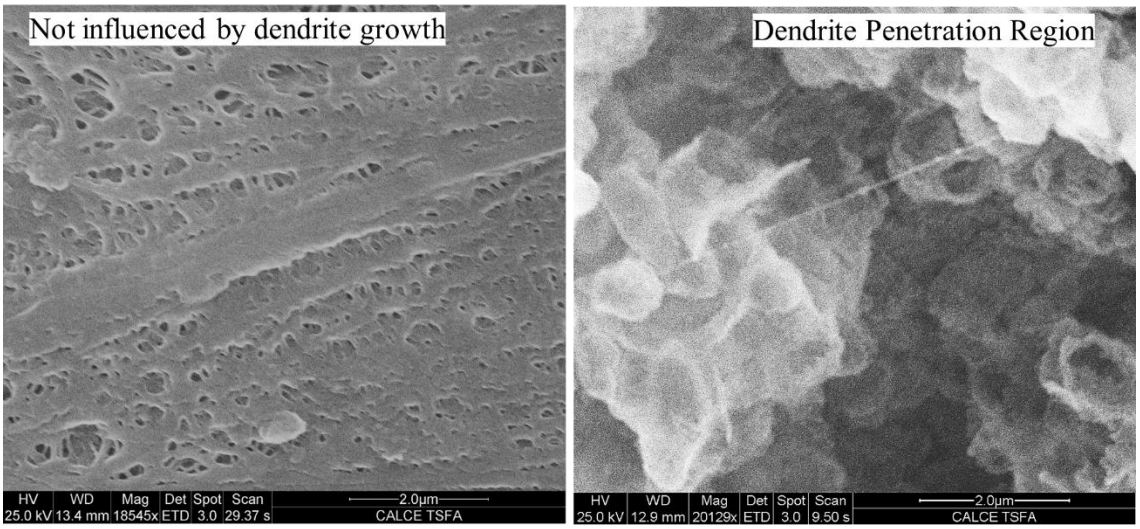

Figure 6.8 Comparison between the unaffected separator and the dendrite penetration region.

The surface morphology of the unaffected separator (Figure 6.9 left) and the dendrite blocking region (Figure 6.9 right) were compared in Figure 6.9. There is no significant difference in their morphologies.

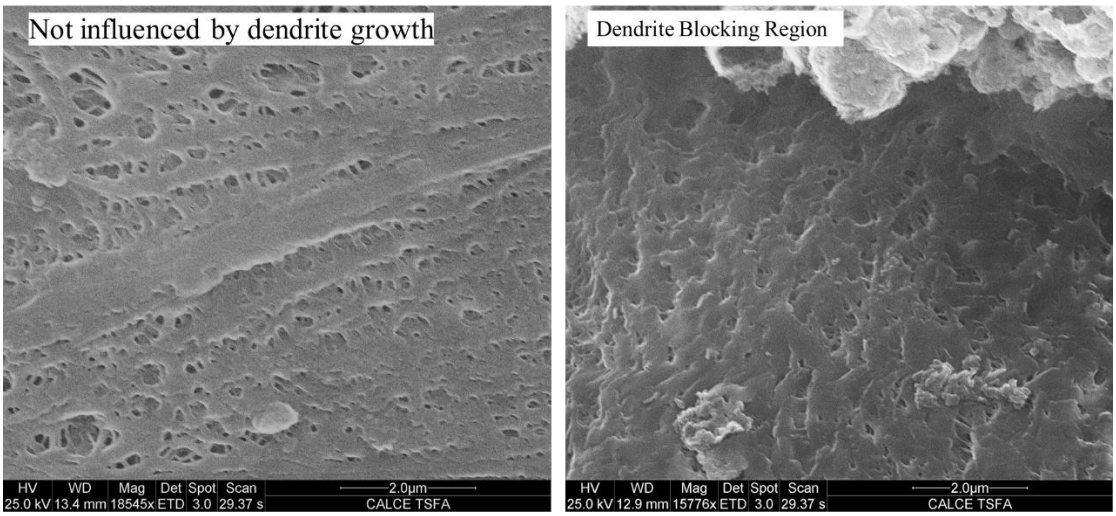

Figure 6.9 Comparison between the unaffected separator and the dendrite blocking region.

Chapter 7: Summary

The lithium dendrite growth under various current densities in two electrolyte systems was examined. Besides, the interaction between the lithium dendrite and separator was also studied. Here summarizes the findings and contributions of the current research work, the limitations of the present work, and the suggestions for future work.

7.1 Findings and contributions of the current research work

Lithium dendrites are a potential root cause of battery short circuits, thermal runaways, fires, and explosions. However, the inability to observe lithium dendrite growth processes makes it challenging to study the growth mechanisms. To facilitate the direct observation of the lithium dendrite growth process, this work modified the design of a transparent cell fixture to incorporate a separator on the electrode to enable: tracking of lithium dendrite growth, evaluating the impact of a separator on dendrite growth, and swift and accurate fabrication and assembly.

Two electrolytes were used in this study: electrolyte A is 1M $LiPF_6$ in EC: DMC (1:1, V:V); electrolyte B is 1.20M $LiPF_6$, EC/PC/EMC=2/1/7 (V:V) 90.5wt% + VC 1.5wt% + FEC 3wt% + PS 2wt% + PST 1wt%+LiDFOB 1wt%+SN 1wt%). Through the LSV test on samples made by two electrolytes, it is identified that electrolyte B has lower limiting current density, exchange current density, and cathodic transfer coefficient. An ideal electrolyte additive should reduce the exchange current density and cathodic transfer coefficient but increase the limiting current density.

The dendrite formed under lower current densities showed lower nucleation sites. The distribution of the dendrite nucleation sites is not uniform, which results in localized dendrite growth. With the increase of initial current density, more dendrite growth spots were formed on the negative electrode, leading to dendrite growth at multiple sites simultaneously.

A morphology transformation in lithium dendrites was identified through the in-situ observation test under various current densities. With the initial current density increase, the lithium dendrite transformed from dense to porous structures. This transition is related to the change in dendrite growing spot. The initial formation of dendrites changed the electrode geometry. It enhanced the electrical field intensity near the tip, which makes this area a preferential growth spot in the following charging process. From the analysis of the average dendrite growth rate under various initial current densities, a generic functional equation was determined, which describes the lithium dendrite growth rate relationship with initial current density.

In-situ observation tests under multiple current densities were conducted in samples with separators covering the negative electrodes. In samples made with electrolyte B, it is found that the dense dendrite formed under low initial current density ($10mA/cm^2$) can tear and penetrate the ultrahigh molecular weight polyethylene (UHMWPE) separator. However, dendrites might also be able to travel through the pores in separators. In contrast, the porous dendrite formed at a high initial current density ($30mA/cm^2$) can be blocked.

7.2 Limitations of the current research work

There are two major limitations in the current work; the sample variation and limited test conditions were included. The lithium dendrite growth is sensitive to the test environment's conditions and the test components' status. In the current study, the sample was manually assembled one by one inside the glovebox, and the components' treatment and assembly accuracy matter. Although the general trend in the average dendrite growth can be seen in the current study, variations in the repeated tests indicate the present study's limitations. Besides the sample variation, the current research work involved only two types of electrolytes and one type of separator. Due to the changes in the solvent, lithium concentration, and additive, there is no direct comparison between the results.

The sample variation is mainly related to the fixture design, which does not strictly limit the position of the two electrodes. The distance between the two electrodes can alter the electric field applied to the negative electrode. Although the distance between the two electrodes was set to be 2 mm in the current study, there are variations in the electrode distance from sample to sample. The dendrite growth process can be accelerated or delayed by varying the distance. Meanwhile, the nucleation status can be changed. Figure 7.1 shows the test conducted in EC: DMC (1:1, V:V) with 1M $LiPF_6$ under 10 mA/cm^2. The electrode distance is set to about 0.5 mm intentionally. Due to the reduced distance between the two electrodes, the electrical field was enhanced, and thus there are more nucleation sites for the dendrite growth. Another issue that originates from the assembly accuracy is how parallel the two electrodes are. This led

to the distance varying inside the same sample. Due to the same reason mentioned above, the electric field can be changed too.

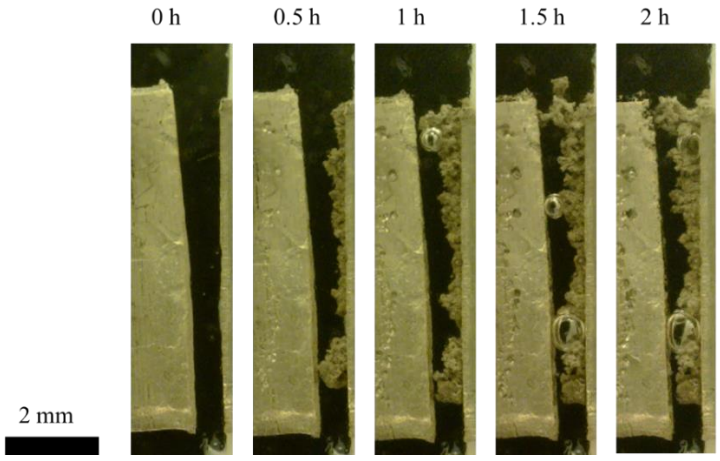

Figure 7.1 Test conducted in EC: DMC with 1M $LiPF_6$ under 10 mA/cm^2. The electrode distance is about 0.5 mm.

Besides the distance variation, the current study uses the front edge of the lithium metal electrode only, while there are comparable amounts of electrodes exposed to the electrolyte simultaneously. Since the reaction area in the current study is not the dominant region, the reactions that occurred in other areas can cause “noise” to the analysis of the test results. For the test with separator implementation, the contact between the separator and the electrode may influence the formed dendrite and the interaction between them.

The electrode preparation process may also introduce variation. The electrode in the current study was prepared through the cold rolling process, in which the electrical

connections between the lithium metal and the copper substrate can vary from one area to the other.

In addition to the sample fabrication and assembly, due to the gas generation and the concentration change in the vicinity of the electrode, convection can be generated inside the current in-situ optical cell, which hinders the application of the dendrite growth at lower current densities. The image shows the dendrite growth in EC: DMC (1:1, V:V) with 1M $LiPF_6$ under 1 mA/cm^2. The formed dendrite grew in the vertical direction instead of the horizontal direction. Thus, in the current research work, no quantitative analysis was conducted on the test conducted at current densities lower than $10mA/cm^2$.

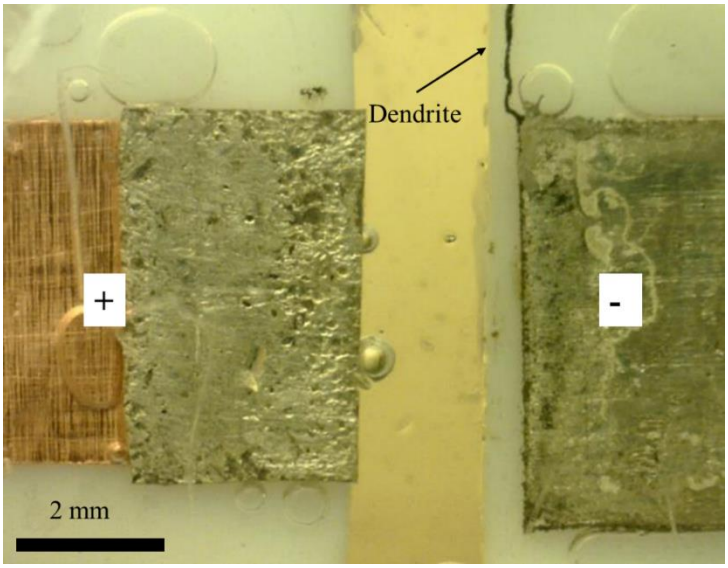

Figure 7.2 Test conducted in EC: DMC with 1M $LiPF_6$ under 1 mA/cm^2.

7.3 Suggestions for future work and potential improvements in fixture design

The limitations mentioned in the previous section also provide opportunities for future lithium dendrite studies. In future work, dendrite growth tests can be conducted with multiple types of separators to compare and analyze the effect of tortuosity on lithium dendrite growth. Besides, dendrite growth tests can be conducted in electrolyte systems with individual ingredients varying at a time to quantify the effect of various electrolyte additives. In addition, the fixture design and assembly process can be improved to address the issues of sample variation. And the dendrite analysis method can also be modified to enable the analysis of the dynamic process of lithium dendrite growth. The last aspects will be discussed in detail in the following two parts.

7.3.1 Improvements in fixture design and assembly

To address the sample-to-sample variation caused by the current fixture design, the surface area will be used for the lithium dendrite growth. At the same time, the influence of other regions can be limited. Figure 7.3 is a demonstration test on a modified electrode setup, where the distance between the two electrodes depends on the spacer's thickness. The improved fixture (Figures 7.4 to 7.6) was designed for consideration. To improve the electrical connections between the lithium metal and the copper current collector, The hot dipping coating process may guarantee a uniform connection between the lithium metal and the copper substrate in future work.

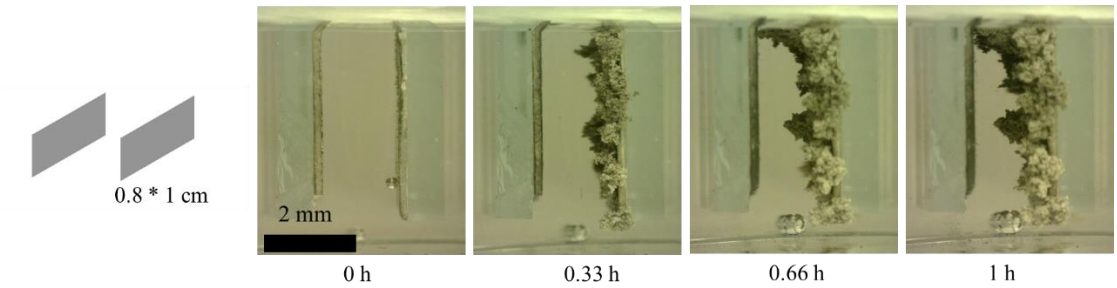

Figure 7.3 Test conducted in EC: DMC with 1M $LiPF_6$ under 10 mA/cm^2. The electrode surface was used for the dendrite growth.

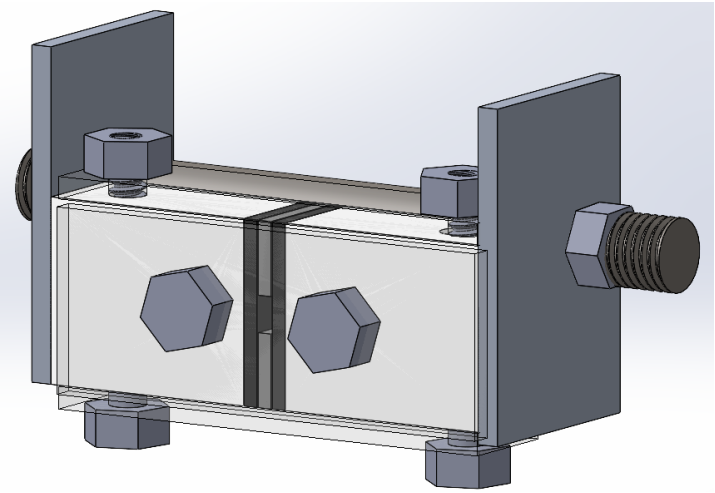

Figure 7.4 Design of 2nd fixture.

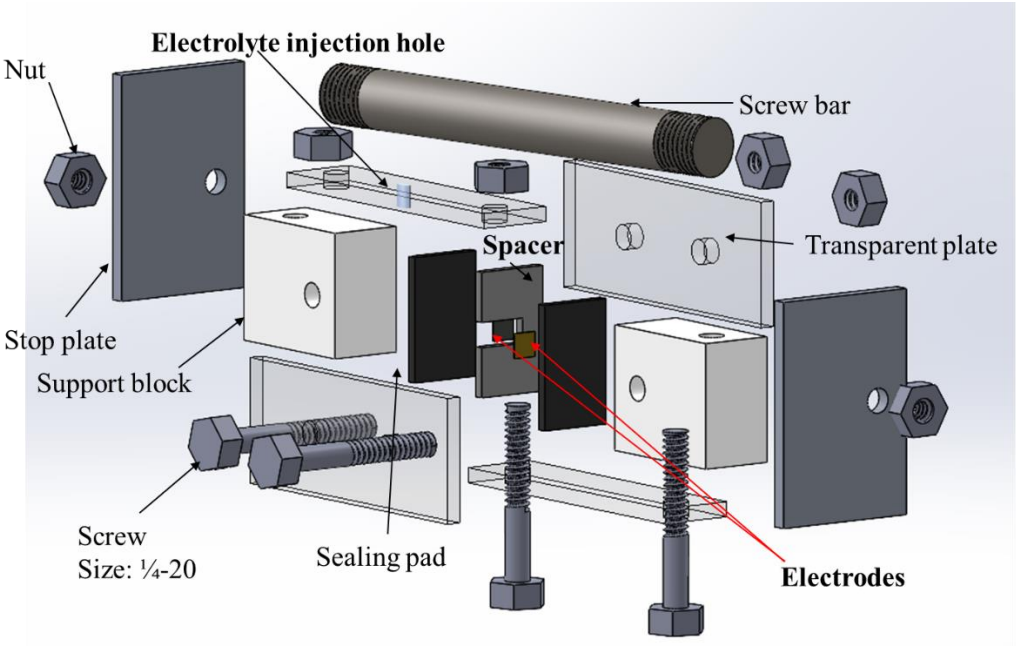

Figure 7.5 Exploded view of the design of 2nd fixture.

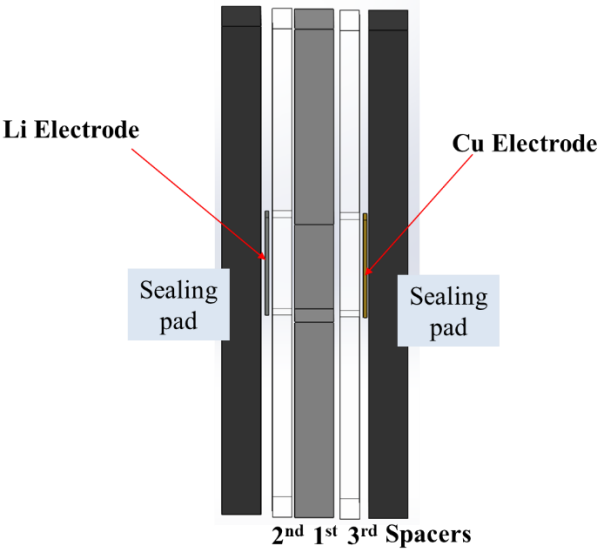

Figure 7.6 Subassembly of the function module.

7.3.2 Improvements in the dendrite analysis method

The current analysis of the dendrite is based on the average dendrite growth rate, which uses only the dendrite length at the end of the test but neglects the dendrite changes during the growth process. Tracking the dendrite change can be a better way to analyze the dendrite growth process. Figure 7.7 demonstrates the application of the modified dendrite analysis method in that the dendrite length was measured every 15 minutes after the beginning of the test.

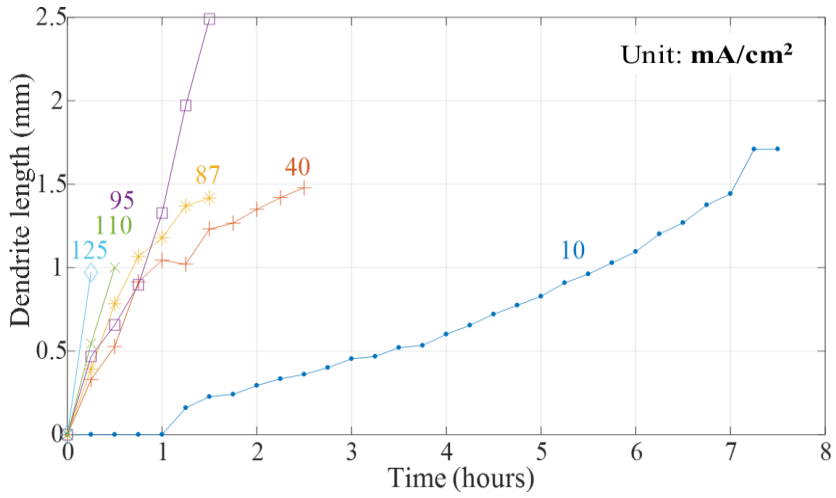

Figure 7.7 The dendrite growth rate over different current densities.

Publications

1. Kong, Lingxi, Yinjiao Xing, and Michael G. Pecht. “In-situ observations of lithium dendrite growth.” IEEE Access 6 (2018): 8387-8393.

2. Kong, Lingxi, Chuan Li, Jiuchun Jiang, and Michael G. Pecht. “Li-ion battery fire hazards and safety strategies.” Energies 11, no. 9 (2018): 2191.

3. Kong, Lingxi, Xiaosong Hu, Guan Gui, Yan Su, and Michael Pecht. “Computed tomography analysis of li-ion battery case ruptures.” Fire technology 56, no. 6 (2020): 2565-2578.

4. Kong, Lingxi, Ryan Aalund, Mohammad Alipour, Stanislav I. Stoliarov, and Michael Pecht. “Evaluating the manufacturing quality of lithium ion pouch batteries.” Journal of The Electrochemical Society 169, no. 4 (2022): 040541.

5. Kong, Lingxi, Diganta Das, and Michael G. Pecht. “The distribution and detection issues of counterfeit lithium-ion batteries.” Energies 15, no. 10 (2022): 3798.

6. Kong, Lingxi, and Michael G. Pecht. “understanding and predicting the risks in li-ion batteries.” In J. F. S. Gomes & S. A. Meguid (Eds.), Proceedings IRF2020: 7th International Conference Integrity-Reliability-Failure. (pp. 587–588) (2020).

7. Saxena, Saurabh, **Lingxi Kong**, and Michael G. Pecht. “Exploding e-cigarettes: A battery safety issue.” IEEE Access 6 (2018): 21442-21466.

8. Sun, Yongquan, **Lingxi Kong**, Hassan Abbas Khan, and Michael G. Pecht. “Li-ion battery reliability–a case study of the Apple iphone®.” IEEE Access 7 (2019): 71131-71141.

9. Yao, Xing-Yan, **Lingxi Kong**, and Michael G. Pecht. “Reliability of cylindrical li-ion battery safety vents.” IEEE Access 8 (2020): 101859-101866.

10. Xu, Bin, **Lingxi Kong**, Guangrui Wen, and Michael G. Pecht. “Protection devices in commercial 18650 lithium-ion batteries.” IEEE Access 9 (2021): 66687-66695.

11. Lingappan, Niranjanmurthi, **Lingxi Kong**, and Michael Pecht. “The significance of aqueous binders in lithium-ion batteries.” Renewable and Sustainable Energy Reviews 147 (2021): 111227.

12. Aalund, Ryan, Weiping Diao, **Lingxi Kong**, and Michael Pecht. “Understanding the non-collision related battery safety risks in electric vehicles a case study in electric vehicle recalls and the LG chem battery.” IEEE Access (2021).

13. Xu, Bin, Jinwoo Lee, Daeil Kwon, **Lingxi Kong**, and Michael Pecht. “Mitigation strategies for Li-ion battery thermal runaway: A review.” Renewable and Sustainable Energy Reviews 150 (2021): 111437.

Bibliography

[1] G. Zhang, X. Wei, X. Tang, J. Zhu, S. Chen, and H. Dai, “Internal short circuit mechanisms, experimental approaches and detection methods of lithium-ion batteries for electric vehicles: A review,” *Renewable and Sustainable Energy Reviews*, vol. 141. Elsevier Ltd, May 01, 2021. doi: 10.1016/j.rser.2021.110790.

[2] Z. Guo, J. Zhu, J. Feng, and S. Du, “Direct in situ observation and explanation of lithium dendrite of commercial graphite electrodes,” *RSC Adv*, vol. 5, no. 85, pp. 69514–69521, Aug. 2015, doi: 10.1039/c5ra13289d.

[3] “Samsung Recalls Galaxy Note7 Smartphones Due to Serious Fire and Burn Hazards,” *U.S. Consumer Product Safety Commission*, Sep. 15, 2016. https://www.cpsc.gov/Recalls/2016/Samsung-Recalls-Galaxy-Note7-Smartphones#:~:text=Recall%20Details&text=This%20recall%20involves%20the%20Samsung,titanium%20with%20a%20matching%20stylus (accessed May 29, 2023).

[4] M. J. Loveridge *et al.*, “Looking deeper into the galaxy (Note 7),” *Batteries*, vol. 4, no. 1, Mar. 2018, doi: 10.3390/batteries4010003.

[5] Y. Yang *et al.*, “A process for combination of recycling lithium and regenerating graphite from spent lithium-ion battery,” *Waste Management*, vol. 85, pp. 529–537, Feb. 2019, doi: 10.1016/j.wasman.2019.01.008.

[6] M. Ue and K. Uosaki, “Recent progress in liquid electrolytes for lithium metal batteries,” *Current Opinion in Electrochemistry*, vol. 17. Elsevier B.V., pp. 106–113, Oct. 01, 2019. doi: 10.1016/j.coelec.2019.05.001.

[7] B. Wu *et al.*, “Li-growth and SEI engineering for anode-free Li-metal rechargeable batteries: A review of current advances,” *Energy Storage Materials*, vol. 57. Elsevier B.V., pp. 508–539, Mar. 01, 2023. doi: 10.1016/j.ensm.2023.02.036.

[8] J.-M. Tarascon and M. Armand, “Issues and challenges facing rechargeable lithium batteries,” 2001. [Online]. Available: www.nature.com

[9] Z. Li, J. Huang, B. Yann Liaw, V. Metzler, and J. Zhang, “A review of lithium deposition in lithium-ion and lithium metal secondary batteries,” *J Power Sources*, vol. 254, pp. 168–182, May 2014, doi: 10.1016/j.jpowsour.2013.12.099.

[10] K. Amine *et al.*, “Nanostructured anode material for high-power battery system in electric vehicles,” *Advanced Materials*, vol. 22, no. 28, pp. 3052–3057, Jul. 2010, doi: 10.1002/adma.201000441.

[11] N. Williard, W. He, C. Hendricks, and M. Pecht, “Lessons learned from the 787 dreamliner issue on Lithium-Ion Battery reliability,” *Energies (Basel)*, vol. 6, no. 9, pp. 4682–4695, 2013, doi: 10.3390/en6094682.

[12] D. Djian, F. Alloin, S. Martinet, H. Lignier, and J. Y. Sanchez, “Lithium-ion batteries with high charge rate capacity: Influence of the porous separator,” *J Power Sources*, vol. 172, no. 1, pp. 416–421, Oct. 2007, doi: 10.1016/j.jpowsour.2007.07.018.

[13] S. P. Kim, A. C. T. V. Duin, and V. B. Shenoy, “Effect of electrolytes on the structure and evolution of the solid electrolyte interphase (SEI) in Li-ion

batteries: A molecular dynamics study," *J Power Sources*, vol. 196, no. 20, pp. 8590–8597, Oct. 2011, doi: 10.1016/j.jpowsour.2011.05.061.

[14] Q. Liu *et al.*, "Understanding undesirable anode lithium plating issues in lithium-ion batteries," *RSC Adv*, vol. 6, no. 91, pp. 88683–88700, 2016, doi: 10.1039/c6ra19482f.

[15] S. A. Han, H. Qutaish, M. S. Park, J. Moon, and J. H. Kim, "Strategic Approaches to the Dendritic Growth and Interfacial Reaction of Lithium Metal Anode," *Chemistry - An Asian Journal*, vol. 16, no. 24. John Wiley and Sons Ltd, pp. 4010–4017, Dec. 13, 2021. doi: 10.1002/asia.202101108.

[16] S. Liu *et al.*, "Crumpled Graphene Balls Stabilized Dendrite-free Lithium Metal Anodes," *Joule*, vol. 2, no. 1, pp. 184–193, Jan. 2018, doi: 10.1016/j.joule.2017.11.004.

[17] J. Steiger, D. Kramer, and R. Mönig, "Mechanisms of dendritic growth investigated by in situ light microscopy during electrodeposition and dissolution of lithium," *J Power Sources*, vol. 261, pp. 112–119, Sep. 2014, doi: 10.1016/j.jpowsour.2014.03.029.

[18] P. Bai, J. Li, F. R. Brushett, and M. Z. Bazant, "Transition of lithium growth mechanisms in liquid electrolytes," *Energy Environ Sci*, vol. 9, no. 10, pp. 3221–3229, Oct. 2016, doi: 10.1039/c6ee01674j.

[19] C. Brissot, M. Rosso, J.-N. Chazalviel, S. Lascaud, and F. Francè´, "Dendritic growth mechanisms in lithium/polymer cells," 1999. [Online]. Available: www.elsevier.comrlocaterjpowsour

[20] I. T. Røe, S. M. Selbach, and S. K. Schnell, “Crystal Structure Influences Migration along Li and Mg Surfaces,” *Journal of Physical Chemistry Letters*, vol. 11, no. 8, pp. 2891–2895, Apr. 2020, doi: 10.1021/acs.jpclett.0c00819.

[21] L. Frenck, G. K. Sethi, J. A. Maslyn, and N. P. Balsara, “Factors That Control the Formation of Dendrites and Other Morphologies on Lithium Metal Anodes,” *Frontiers in Energy Research*, vol. 7. Frontiers Media S.A., Nov. 01, 2019. doi: 10.3389/fenrg.2019.00115.

[22] C. H. Chen and C. W. Pao, “Phase-field study of dendritic morphology in lithium metal batteries,” *J Power Sources*, vol. 484, Feb. 2021, doi: 10.1016/j.jpowsour.2020.229203.

[23] X. Zhang *et al.*, “Rethinking How External Pressure Can Suppress Dendrites in Lithium Metal Batteries,” *J Electrochem Soc*, vol. 166, no. 15, pp. A3639–A3652, 2019, doi: 10.1149/2.0701914jes.

[24] X. Gao *et al.*, “Thermodynamic Understanding of Li-Dendrite Formation,” *Joule*, vol. 4, no. 9. Cell Press, pp. 1864–1879, Sep. 16, 2020. doi: 10.1016/j.joule.2020.06.016.

[25] D. R. Ely and R. E. García, “Heterogeneous Nucleation and Growth of Lithium Electrodeposits on Negative Electrodes,” *J Electrochem Soc*, vol. 160, no. 4, pp. A662–A668, 2013, doi: 10.1149/1.057304jes.

[26] A. Aryanfar, D. J. Brooks, A. J. Colussi, B. V. Merinov, W. A. Goddard, and M. R. Hoffmann, “Thermal relaxation of lithium dendrites,” *Physical Chemistry Chemical Physics*, vol. 17, no. 12, pp. 8000–8005, Mar. 2015, doi: 10.1039/c4cp05786d.

[27] C. T. Love, O. A. Baturina, and K. E. Swider-Lyons, “Observation of lithium dendrites at ambient temperature and below,” *ECS Electrochemistry Letters*, vol. 4, no. 2, pp. A24–A27, 2014, doi: 10.1149/2.0041502eel.

[28] X. Wang, Y. Hou, Y. Zhu, Y. Wu, and R. Holze, “An Aqueous Rechargeable Lithium Battery Using Coated Li Metal as Anode,” *Sci Rep*, vol. 3, 2013, doi: 10.1038/srep01401.

[29] A. A. Arie and J. K. Lee, “Electrochemical characteristics of lithium metal anodes with diamond like carbon film coating layer,” *Diam Relat Mater*, vol. 20, no. 3, pp. 403–408, Mar. 2011, doi: 10.1016/j.diamond.2011.01.040.

[30] S. H. Kim, K. H. Choi, S. J. Cho, E. H. Kil, and S. Y. Lee, “Mechanically compliant and lithium dendrite growth-suppressing composite polymer electrolytes for flexible lithium-ion batteries,” *J Mater Chem A Mater*, vol. 1, no. 16, pp. 4949–4955, Apr. 2013, doi: 10.1039/c3ta10612h.

[31] S. K. Jeong *et al.*, “Suppression of dendritic lithium formation by using concentrated electrolyte solutions,” *Electrochem commun*, vol. 10, no. 4, pp. 635–638, Apr. 2008, doi: 10.1016/j.elecom.2008.02.006.

[32] A. Aryanfar, D. J. Brooks, A. J. Colussi, B. V. Merinov, W. A. Goddard, and M. R. Hoffmann, “Thermal relaxation of lithium dendrites,” *Physical Chemistry Chemical Physics*, vol. 17, no. 12, pp. 8000–8005, Mar. 2015, doi: 10.1039/c4cp05786d.

[33] R. Akolkar, “Modeling dendrite growth during lithium electrodeposition at sub-ambient temperature,” *J Power Sources*, vol. 246, pp. 84–89, 2014, doi: 10.1016/j.jpowsour.2013.07.056.

[34] R. Akolkar, “Mathematical model of the dendritic growth during lithium electrodeposition,” *J Power Sources*, vol. 232, pp. 23–28, 2013, doi: 10.1016/j.jpowsour.2013.01.014.

[35] F. Orsini *et al.*, “In situ Scanning Electron Microscopy SEM observation of interfaces within plastic lithium batteries ′ ′ ′ ′,” 1998.

[36] I. W. Seong, C. H. Hong, B. K. Kim, and W. Y. Yoon, “The effects of current density and amount of discharge on dendrite formation in the lithium powder anode electrode,” *J Power Sources*, vol. 178, no. 2, pp. 769–773, Apr. 2008, doi: 10.1016/j.jpowsour.2007.12.062.

[37] X. B. Cheng, R. Zhang, C. Z. Zhao, F. Wei, J. G. Zhang, and Q. Zhang, “A review of solid electrolyte interphases on lithium metal anode,” *Advanced Science*, vol. 3, no. 3, Nov. 2016, doi: 10.1002/advs.201500213.

[38] Y. Liu, D. Lin, Z. Liang, J. Zhao, K. Yan, and Y. Cui, “Lithium-coated polymeric matrix as a minimum volume-change and dendrite-free lithium metal anode,” *Nat Commun*, vol. 7, Mar. 2016, doi: 10.1038/ncomms10992.

[39] X. B. Cheng, R. Zhang, C. Z. Zhao, F. Wei, J. G. Zhang, and Q. Zhang, “A review of solid electrolyte interphases on lithium metal anode,” *Advanced Science*, vol. 3, no. 3, Nov. 2015, doi: 10.1002/advs.201500213.

[40] G. Ramos-Sanchez *et al.*, “Computational studies of interfacial reactions at anode materials: Initial stages of the solid-electrolyte-interphase layer formation,” *Journal of Electrochemical Energy Conversion and Storage*, vol. 13, no. 3, Aug. 2016, doi: 10.1115/1.4034412.

[41] C. Barchasz, J.-C. Leprêtre, S. Patoux, and F. Alloin, “Revisiting TEGDME/DIOX Binary Electrolytes for Lithium/Sulfur Batteries: Importance of Solvation Ability and Additives,” *J Electrochem Soc*, vol. 160, no. 3, pp. A430–A436, 2013, doi: 10.1149/2.022303jes.

[42] Q. Li, J. Chen, L. Fan, X. Kong, and Y. Lu, “Progress in electrolytes for rechargeable Li-based batteries and beyond,” *Green Energy and Environment*, vol. 1, no. 1. KeAi Publishing Communications Ltd., pp. 18–42, Apr. 01, 2016. doi: 10.1016/j.gee.2016.04.006.

[43] J. Zheng *et al.*, “Highly Stable Operation of Lithium Metal Batteries Enabled by the Formation of a Transient High-Concentration Electrolyte Layer,” *Adv Energy Mater*, vol. 6, no. 8, Apr. 2016, doi: 10.1002/aenm.201502151.

[44] I. Belharouak, G. M. Koenig, and K. Amine, “Electrochemistry and safety of Li4Ti5O12 and graphite anodes paired with LiMn2O4 for hybrid electric vehicle Li-ion battery applications,” *J Power Sources*, vol. 196, no. 23, pp. 10344–10350, Dec. 2011, doi: 10.1016/j.jpowsour.2011.08.079.

[45] S. S. Zhang, “A review on electrolyte additives for lithium-ion batteries,” *Journal of Power Sources*, vol. 162, no. 2 SPEC. ISS. Elsevier, pp. 1379–1394, Nov. 22, 2006. doi: 10.1016/j.jpowsour.2006.07.074.

[46] S. Liu *et al.*, “Effect of co-doping nano-silica filler and N-methyl-N-propylpiperidinium bis(trifluoromethanesulfonyl)imide into polymer electrolyte on Li dendrite formation in Li/poly(ethylene oxide)-Li(CF3SO2) 2N/Li,” *J Power Sources*, vol. 196, no. 18, pp. 7681–7686, Sep. 2011, doi: 10.1016/j.jpowsour.2011.04.001.

[47] R. Mogi, M. Inaba, S.-K. Jeong, Y. Iriyama, T. Abe, and Z. Ogumi, “Effects of Some Organic Additives on Lithium Deposition in Propylene Carbonate,” *J Electrochem Soc*, vol. 149, no. 12, p. A1578, 2002, doi: 10.1149/1.1516770.

[48] S. P. Kim, A. C. T. V. Duin, and V. B. Shenoy, “Effect of electrolytes on the structure and evolution of the solid electrolyte interphase (SEI) in Li-ion batteries: A molecular dynamics study,” *J Power Sources*, vol. 196, no. 20, pp. 8590–8597, Oct. 2011, doi: 10.1016/j.jpowsour.2011.05.061.

[49] H. H. Lee, Y. Y. Wang, C. C. Wan, M. H. Yang, H. C. Wu, and D. T. Shieh, “The function of vinylene carbonate as a thermal additive to electrolyte in lithium batteries,” *J Appl Electrochem*, vol. 35, no. 6, pp. 615–623, Jun. 2005, doi: 10.1007/s10800-005-2700-x.

[50] G. Gnana Kumar, K. Reddy, K. S. Nahm, N. Angulakshmi, and A. Manuel Stephan, “Synthesis and electrochemical properties of SnS as possible anode material for lithium batteries,” *Journal of Physics and Chemistry of Solids*, vol. 73, no. 9, pp. 1187–1190, Sep. 2012, doi: 10.1016/j.jpcs.2012.04.013.

[51] B. S. Parimalam, A. D. MacIntosh, R. Kadam, and B. L. Lucht, “Decomposition Reactions of Anode Solid Electrolyte Interphase (SEI) Components with LiPF6,” *Journal of Physical Chemistry C*, vol. 121, no. 41, pp. 22733–22738, Oct. 2017, doi: 10.1021/acs.jpcc.7b08433.

[52] W. Zhang *et al.*, “Tuning the LUMO Energy of an Organic Interphase to Stabilize Lithium Metal Batteries,” *ACS Energy Lett*, vol. 4, no. 3, pp. 644–650, Mar. 2019, doi: 10.1021/acsenergylett.8b02483.

[53] J. Tan, J. Matz, P. Dong, J. Shen, and M. Ye, “A Growing Appreciation for the Role of LiF in the Solid Electrolyte Interphase,” *Advanced Energy Materials*. John Wiley and Sons Inc, 2021. doi: 10.1002/aenm.202100046.

[54] D. Bar-Tow, E. Peled, and L. Burstein, “A Study of Highly Oriented Pyrolytic Graphite as a Model for the Graphite Anode in Li-Ion Batteries,” 1999.

[55] F. Lindgren *et al.*, “SEI Formation and Interfacial Stability of a Si Electrode in a LiTDI-Salt Based Electrolyte with FEC and VC Additives for Li-Ion Batteries,” *ACS Appl Mater Interfaces*, vol. 8, no. 24, pp. 15758–15766, Jun. 2016, doi: 10.1021/acsami.6b02650.

[56] M. Lu, H. Cheng, and Y. Yang, “A comparison of solid electrolyte interphase (SEI) on the artificial graphite anode of the aged and cycled commercial lithium ion cells,” *Electrochim Acta*, vol. 53, no. 9, pp. 3539–3546, Mar. 2008, doi: 10.1016/j.electacta.2007.09.062.

[57] P. G. Kitz, M. J. Lacey, P. Novák, and E. J. Berg, “Influence of VC and FEC Additives on Interphase Properties of Carbon in Li-ion Cells Investigated by Combined EIS & EQCM-D.”

[58] P. Verma, P. Maire, and P. Novák, “A review of the features and analyses of the solid electrolyte interphase in Li-ion batteries,” *Electrochimica Acta*, vol. 55, no. 22. pp. 6332–6341, Sep. 01, 2010. doi: 10.1016/j.electacta.2010.05.072.

[59] Y. Xu *et al.*, “Atomic to Nanoscale Origin of Vinylene Carbonate Enhanced Cycling Stability of Lithium Metal Anode Revealed by Cryo-Transmission

Electron Microscopy," *Nano Lett*, vol. 20, no. 1, pp. 418–425, Jan. 2020, doi: 10.1021/acs.nanolett.9b04111.

[60] P. Lu, C. Li, E. W. Schneider, and S. J. Harris, "Chemistry, impedance, and morphology evolution in solid electrolyte interphase films during formation in lithium ion batteries," *Journal of Physical Chemistry C*, vol. 118, no. 2, pp. 896–903, Jan. 2014, doi: 10.1021/jp4111019.

[61] Y. Zhou *et al.*, "Real-time mass spectrometric characterization of the solid–electrolyte interphase of a lithium-ion battery," *Nat Nanotechnol*, vol. 15, no. 3, pp. 224–230, Mar. 2020, doi: 10.1038/s41565-019-0618-4.

[62] A. Mistry, C. Fear, R. Carter, C. T. Love, and P. P. Mukherjee, "Electrolyte Confinement Alters Lithium Electrodeposition," *ACS Energy Lett*, vol. 4, no. 1, pp. 156–162, Jan. 2019, doi: 10.1021/acsenergylett.8b02003.

[63] X. Huang, "Separator technologies for lithium-ion batteries," *Journal of Solid State Electrochemistry*, vol. 15, no. 4. pp. 649–662, Apr. 2011. doi: 10.1007/s10008-010-1264-9.

[64] C. T. Love, "Perspective on the mechanical interaction between lithium dendrites and polymer separators at low temperature," *Journal of Electrochemical Energy Conversion and Storage*, vol. 13, no. 3, Aug. 2016, doi: 10.1115/1.4034483.

[65] A. Jana, D. R. Ely, and R. E. García, "Dendrite-separator interactions in lithium-based batteries," *J Power Sources*, vol. 275, pp. 912–921, Feb. 2015, doi: 10.1016/j.jpowsour.2014.11.056.

[66] P. Bai *et al.*, “Interactions between Lithium Growths and Nanoporous Ceramic Separators,” *Joule*, vol. 2, no. 11, pp. 2434–2449, Nov. 2018, doi: 10.1016/j.joule.2018.08.018.

[67] H. Wu, D. Zhuo, D. Kong, and Y. Cui, “Improving battery safety by early detection of internal shorting with a bifunctional separator,” *Nat Commun*, vol. 5, Oct. 2014, doi: 10.1038/ncomms6193.

[68] T. Nishida, K. Nishikawa, M. Rosso, and Y. Fukunaka, “Optical observation of Li dendrite growth in ionic liquid,” *Electrochim Acta*, vol. 100, pp. 333–341, Jun. 2013, doi: 10.1016/j.electacta.2012.12.131.

[69] H. J. Chang *et al.*, “Investigating Li Microstructure Formation on Li Anodes for Lithium Batteries by in Situ 6Li/7Li NMR and SEM,” *Journal of Physical Chemistry C*, vol. 119, no. 29, pp. 16443–16451, Jul. 2015, doi: 10.1021/acs.jpcc.5b03396.

[70] A. Aryanfar, D. J. Brooks, A. J. Colussi, and M. R. Hoffmann, “Quantifying the dependence of dead lithium losses on the cycling period in lithium metal batteries,” *Physical Chemistry Chemical Physics*, vol. 16, no. 45, pp. 24965–24970, Oct. 2014, doi: 10.1039/c4cp03590a.

[71] N. Schweikert *et al.*, “Suppressed lithium dendrite growth in lithium batteries using ionic liquid electrolytes: Investigation by electrochemical impedance spectroscopy, scanning electron microscopy, and in situ 7Li nuclear magnetic resonance spectroscopy,” *J Power Sources*, vol. 228, pp. 237–243, 2013, doi: 10.1016/j.jpowsour.2012.11.124.

[72] W. Li *et al.*, “The synergetic effect of lithium polysulfide and lithium nitrate to prevent lithium dendrite growth,” *Nat Commun*, vol. 6, Jun. 2015, doi: 10.1038/ncomms8436.

[73] S. Tippmann, D. Walper, L. Balboa, B. Spier, and W. G. Bessler, “Low-temperature charging of lithium-ion cells part I: Electrochemical modeling and experimental investigation of degradation behavior,” *J Power Sources*, vol. 252, pp. 305–316, Apr. 2014, doi: 10.1016/j.jpowsour.2013.12.022.

[74] F. Sagane, K. I. Ikeda, K. Okita, H. Sano, H. Sakaebe, and Y. Iriyama, “Effects of current densities on the lithium plating morphology at a lithium phosphorus oxynitride glass electrolyte/copper thin film interface,” *J Power Sources*, vol. 233, pp. 34–42, 2013, doi: 10.1016/j.jpowsour.2013.01.051.

[75] C. T. Love, “Thermomechanical analysis and durability of commercial micro-porous polymer Li-ion battery separators,” *J Power Sources*, vol. 196, no. 5, pp. 2905–2912, Mar. 2011, doi: 10.1016/j.jpowsour.2010.10.083.

[76] L. Kong, Y. Xing, and M. G. Pecht, “In-Situ Observations of Lithium Dendrite Growth,” *IEEE Access*, vol. 6, 2018, doi: 10.1109/ACCESS.2018.2805281.

[77] M. Dollé, L. Sannier, B. Beaudoin, M. Trentin, and J. M. Tarascon, “Live scanning electron microscope observations of dendritic growth in lithium/polymer cells,” *Electrochemical and Solid-State Letters*, vol. 5, no. 12, Dec. 2002, doi: 10.1149/1.1519970.

[78] P. Biswal, S. Stalin, A. Kludze, S. Choudhury, and L. A. Archer, “Nucleation and Early Stage Growth of Li Electrodeposits,” *Nano Lett*, vol. 19, no. 11, pp. 8191–8200, Nov. 2019, doi: 10.1021/acs.nanolett.9b03548.

[79] A. Jana, S. I. Woo, K. S. N. Vikrant, and R. E. García, "Electrochemomechanics of lithium dendrite growth," *Energy Environ Sci*, vol. 12, no. 12, pp. 3595–3607, Dec. 2019, doi: 10.1039/c9ee01864f.